Microstructure informed micromechanical modelling of hydrated cement paste
Techniques and challenges

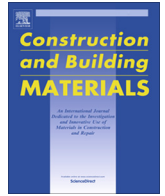Zhang, Hongzhi; Xu, Yading; Gan, Yidong; Chang, Ze; Schlangen, Erik; Šavija, Branko

Important note
To cite this publication, please use the final published version (if applicable).
Please check the document version above.

Microstructure informed micromechanical modelling of hydrated cement paste: Techniques and challenges

Hongzhi Zhang [a,b], Yading Xu [a,*], Yidong Gan [a], Ze Chang [a], Erik Schlangen [a], Branko Šavija [a]

[a] Faculty of Civil Engineering and Geosciences, Delft University of Technology, 2628 CN Delft, the Netherlands
[b] School of Qilu Transportation, Shandong University, 250002 Jinan, PR China

HIGHLIGHTS

- A review on microstructure characterization of cement paste has been given.
- Reviewed approaches for assessing the mechanical properties of individual phases.
- Approaches on micromechanical modelling of cement paste has been reviewed.
- Basic Principles and corresponding results are given for the reviewed techniques.

ARTICLE INFO

ABSTRACT

Application of micromechanical modelling of hydrated cement paste (HCP) gains more and more interests in the field of cementitious materials. One of the most promising approaches is the use of so-called microstructure informed micromechanical models, which provides a direct link between microstructure and mechanical properties. In order to properly model the micromechanical properties of HCP, advanced mechanical models, well-characterised microstructures and proper input parameters are required. However, due to the complex material structure of HCP, this is not an easy to achieve for any of the three aforementioned aspects. Therefore, this paper aims at reviewing of the techniques that have been developed to contribute to the micromechanical modelling. Basic principles, corresponding research results, recent advances and limitations are given. It is expected that this review can help researchers make reasonable choices on techniques for the micromechanical modelling of cementitious materials.

Contents

* Corresponding author.
  E-mail addresses: hzzhang@sdu.end.cn (H. Zhang), Y.Xu-5@tudelft.nl (Y. Xu), Y.Gan@tudelft.nl (Y. Gan), Z.Chang-1@tudelft.nl (Z. Chang), erik.schlangen@tudelft.nl (E. Schlangen), b.savija@tudelft.nl (B. Šavija).

1. Introduction

Hydrated cement paste (HCP) is formed by the reaction of Portland cement clinker with water. As the main binder material of concrete, its mechanical properties such as strength and elastic modulus are of significant importance for the properties of this composite material [1–3]. Accurate prediction of concrete properties therefore depends, to a large extent, on good understanding of behaviour of HCP. Therefore, simulation and prediction of HCP mechanical properties form a major topic of research in the field of cementitious materials.

It is generally accepted that the critical length scale for studying HCP is the micro-scale, as the micro-scale corresponds to the length scale where constituents, most importantly calcium silicate hydrate (C-S-H), calcium hydroxide (CH), anhydrous cement clinker and capillary pores, can be distinguished. In pursuit of fundamental understanding of the link between the microstructure and its macroscopic mechanical performance, mechanical models using microstructural information as input are generally used. Such models are therefore considered to be microstructure-informed. In the past decade or so, numerous microstructure-informed models have been proposed. In general, these models comprise three steps:

- The first step is to obtain a realistic microstructure, which is the basis for determining the properties of a material. This can be achieved with the aid of either experimental techniques, e.g. scanning electron microscopy (SEM) [4] and X-ray computed microtomography (μCT) [5], or numerical models, e.g. Hymostruc [6–8], μic [9,10] and CemHyd3D [11], etc.
- The second step is to determine the local micromechanical properties of different phases. Usually micromechanical properties of different phases are derived from nano-indentation measurements [12–15]. An alternative is to use atomistic simulations [16,17].
- Once the microstructure and the local micromechanical properties are available, the microstructure-informed modelling models can be used. Using such models, mechanical properties of the material can be determined.

This paper aims at reviewing techniques that are related with the aforementioned three aspects. Basic principles, corresponding research results, recent advances and limitations are given for the reviewed techniques. It is expected that with the provided review, a clear understanding for micromechanical modelling of hydrated cement paste would be achieved. Perspectives for further developments in the future are outlined. These techniques can be further developed and applied to understand the micromechanical properties of the other binder materials such as blended cement pastes, recycled materials and geopolymers. This helps developing more durable and sustainable construction materials.

2. Microstructure characterization

2.1. Experimental approach

In terms of visualisation of cement paste, experimental techniques including SEM [4], μCT [5], scanning laser scanning confocal microscopy [18,19], focused ion beam nanotomography [20,21], or scanning transmission X-ray microscopy [22,23] can be applied. Among those, SEM and μCT are the most widely used techniques. The initial outcomes from these two approaches are greyscale level images. Using image segmentation and thresholding techniques, the morphology and spatial distribution of individual phases in the HCP can be derived. These play a crucial role for the micromechanical modelling.

2.1.1. Scanning electron microscopy (SEM)

During the last 30 years, scanning electron microscope has become a general and versatile instrument for studying the microstructure of hardened cement paste. SEM produces images of a sample by scanning the surface with a focused beam of electrons and collecting the signals from the interaction between electrons and atoms on the material surface. As shown in Fig. 1, the following three modes can be classified in terms of the type of the signal that used for the imaging:

- The secondary electron (SE) mode collects low-energy secondary electrons originating within a few nanometers from the sample surface [24]. This mode results in images with a well-defined, three-dimensional appearance, which is commonly used to observe individual particles, fracture surfaces or hydrate surface.
- Backscattered electrons (BSE) consist of high-energy electrons originating in the electron beam. The detection of such electrons allows visualization of contrast between areas with
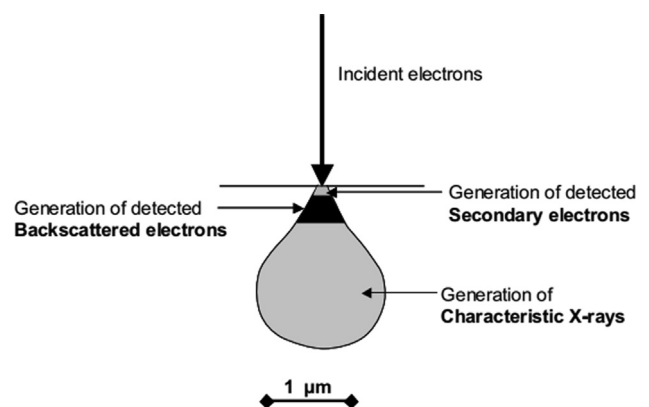

Fig. 1. Schematic view of signal generation in scanning electron microscope [4].

different chemical compositions [24]. This is because the heavy elements (high atomic number) backscatter electrons more strongly than light elements (low atomic number), and thus appear brighter in the image. The BSE image can be used for quantification of spatial distribution and amount of different microstructural constituents in hardened cement paste matrix.

- The analysis of characteristic X-rays generated throughout the interaction volume energy-dispersive gives the chemical composition of the local area [24]. Energy dispersive spectroscopy (EDS) or wavelength dispersive spectroscopy (WDS) are generally used for this purpose.

In order to build the microstructure - property relationships, it is necessary to quantify the microstructural features. For this purpose, BSE imaging is combined with image segmentation techniques or EDS mapping. Prior to the BSE imaging, the cement paste sample is impregnated with low viscosity epoxy and well-polished. A typical BSE image of a cement paste surface is shown in Fig. 2a. The anhydrous cement clinker particles are the brightest; the calcium hydroxide (CH) looks lighter grey and other hydration products (e.g. calcium-silicate-hydrate, C-S-H) are as various shades of darker grey. Due to the low average atomic number of the epoxy that is filling the pores, the pores do not scatter electrons and appear black in BSE images. Such contrast between different features offers an opportunity for image segmentation, see Fig. 2. A typical grey-level histogram of hardened cement paste is shown in Fig. 3. In the histogram, several peaks can be observed. From right to left, these peaks correspond to anhydrous cement particles, CH and C-S-H, respectively. It needs to be emphasized that no distinct peak for porosity occurs in the histogram. This is partly due to the resolution of the BSE technique and partly due to the limited boundary resolution [4]. Several strategies have been proposed to determine the threshold between pore and C-S-H. Depending on whether the histogram (Fig. 3) or cumulative curve of the greyscale level (Fig. 4) is used, the tangent-slope method [25] or the "overflow" pore segmentation method [26], respectively, is commonly applied. Although reasonable correlation with other measures of porosity and pore size distribution can be obtained [8], it should be noticed that when these strategies are used, the areas containing solid intermixed pores could be merged as solid or pore phases depending on the internal porosity of the local area. Furthermore, it is worth noticing that drying and specimen preparation for the BSE examination could introduce irreversible changes in the pore structure [5]. An environmental electron microscope (ESEM) can be used to overcome the issue of specimen drying under vacuum. However, polishing is still required during the specimen preparation.

Fig. 3. Typical greyscale level histogram of hardened cement paste. From the right (highest grey levels) the peaks correspond to anhydrous cement particles, CH and C-S-H respectively. No discrete peak for porosity is observed [4].
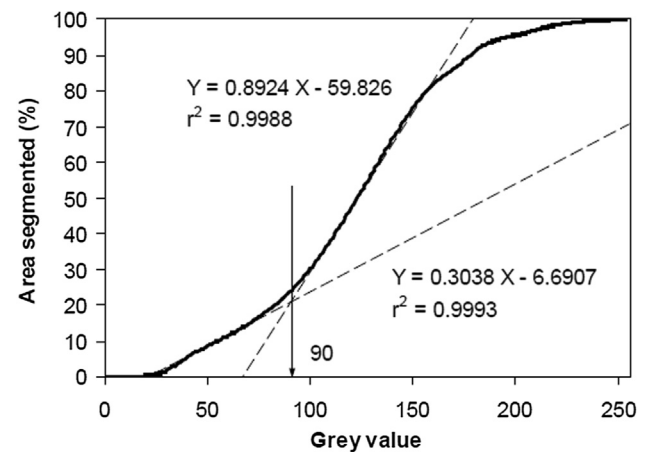
Fig. 4. Determination of the "overflow" point for the pore segmentation using the cumulative greyscale histogram after [26].

As mentioned above, because of the limitation of the resolution, a single pixel in a BSE image can contain signals from several phases, and relatively broad individual peaks are usually observed in the histogram (Fig. 3). EDS mapping can be coupled with the BSE technique to get the detailed chemical quantification of the
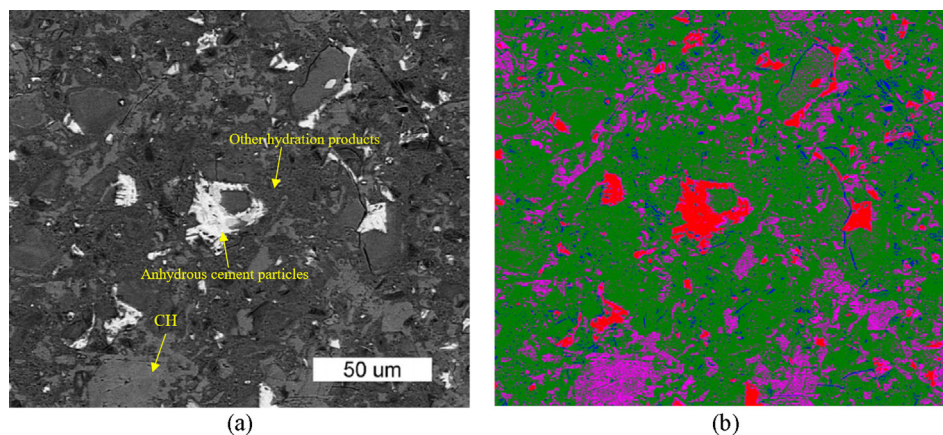

Fig. 2. An example of a segmented SEM image of hydrated cement paste: (a) original BSE image; (b) segmented image (blue = pores; green + violet = hydrates (violet = large CH crystals as a part of hydrates); red = anhydrous cement particles) after [27]. (For interpretation of the references to colour in this figure legend, the reader is referred to the web version of this article.)
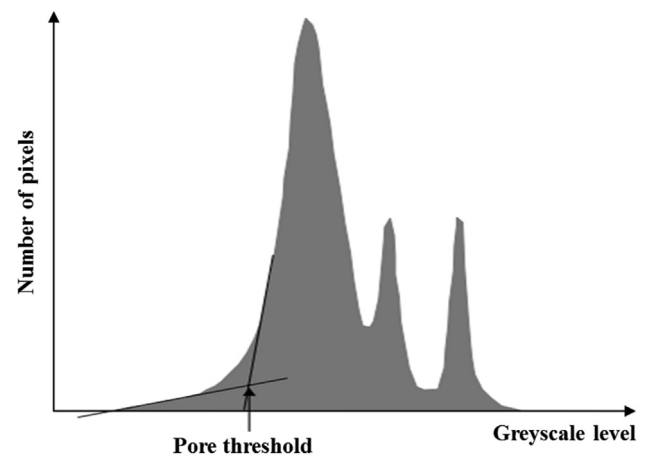
Fig. 5. Schematic illustration of the image acquisition sequence for the 3D reconstruction of the samples analysed by x-ray computed tomography [29].

hydrated matrix. In terms of identifying the hydration products, Al-Si-Ca system is of main interest.

Although BSE technique has offered a lot of valuable knowledge for understanding the features of cementitious materials at the micro scale, it should be kept in mind that it can only offer two-dimensional (2D) section observations of a three-dimensional (3D) microstructure. This leads the challenge to the techniques for transforming 2D information to 3D. For example, quantitative parameters, such as overall volume fractions of a phase can be well estimated from 2 D sections, but parameters like pore connectivity can be difficult to assess.

2.1.2. X-ray computed microtomography (μCT)

Due to the ease of sample preparation and its non-destructive character, X-ray computed tomography has become an attractive technique for acquiring a 3D microstructure of cementitious materials. As schematically shown in Fig. 5, an object is placed between an X-ray source and a detector. By rotating the sample, a series of 2D projections is created on the basis of measuring transmitted intensities by the detector. These projections are then used for the reconstruction of the 3D material stru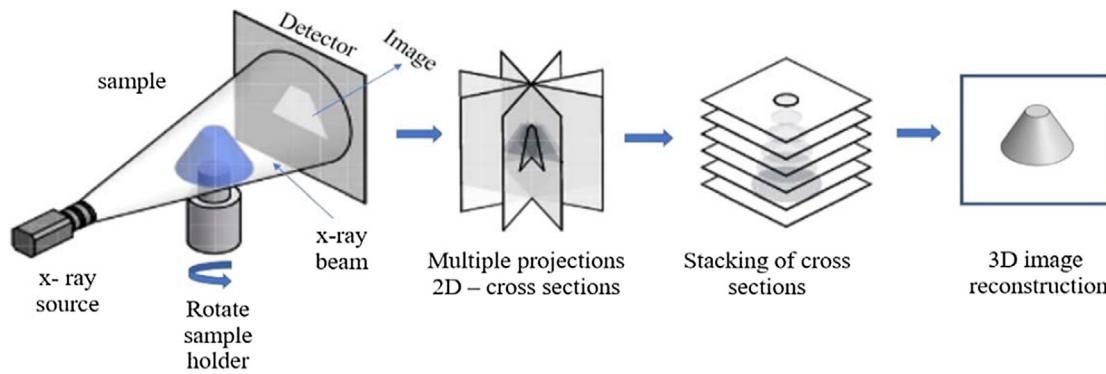cture. The detected intensity I during X-ray irradiation is related to the integral attenuation of the various materials found inside the object following Lambert-Beer Law [28]:

$$I = I_0 e^{(-\mu t)} \tag{1}$$

where I_0 is the intensity of the incident radiation, t the thickness of the object and μ the attenuation coefficient of the object, in which the attenuation coefficient is a function of the density and the atomic number of the scanned object. After reconstruction, a stack of greyscale level based cross-section images of the physical object can be obtained.

In 1990–2000, pioneering work has been conducted on construction materials using conventional X-ray tomography [30-33]. The resolution is limited, thus only large-scale features can be observed. With application of the synchrotron microtomography technique, the capabilities of the tomography systems have increased, making it possible to obtain a 3D material structure of hardened cement paste with a resolution better than 0.5 μm [34-36]. This resolution allows a direction observation of the material features of cementitious materials at the micrometre length scale. First tomographic scans of cement pastes are reported by Bentz *et al.* [37].Various microstructures of hardened cement paste with high spatial resolution (0.95 μm per voxel) are available on the Visible Cement Data Set website (https://visiblecement.nist.gov/). Further work was done by Gallucci *et al.* [5], who compared a reconstructed slice from μCT with a BSE image acquired at equivalent magnification, see Fig. 6. They concluded that similar phase
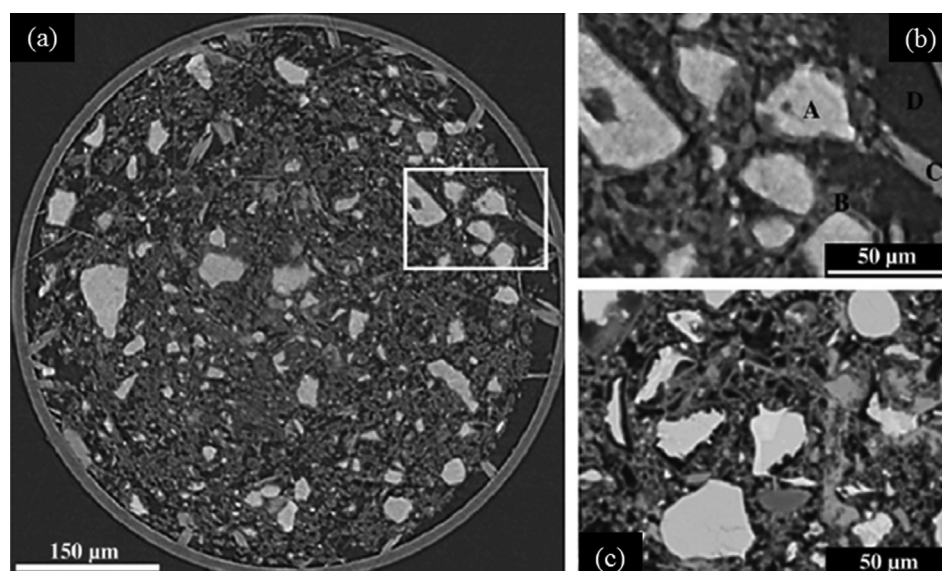

Fig. 6. (a) Reconstructed slice of a 1-day old cement paste; (b) zoomed part of rectangle in (a); (c) comparison with similar specimen in SEM. A-anhydrous cement grains, B-inner C-S-H, C-CH, D-unfilled spaces (air or water filled porosity) [5].

contrast is made for these two techniques, although the beam–matter interactions are fundamentally different. The anhydrous cement particles (A) appear as the brightest phase; 'inner' C-S-H and undifferentiated hydration products (B) are grey; CH shows (C) light grey and pore (D) the darkest phase. As the image resolution partly depends on the size of the scanned specimens, small sized specimen is required. This is generally achieved by injecting the fresh mixture into a plastic tube with diameter around a few hundred micrometres [5,34–36]. However, this approach has difficulties with preparing mixtures have a low w/c ratio. Therefore, the reported results in the literature are mostly based on the high w/c ratio specimens, typically 0.5. The possible way to solve this problem may be cutting or drilling the small pieces material from the hydrated "big" specimens using advanced cutting tools. The authors have recently adopted a micro-dicing saw which was originally used in semi-conductor industry to cut small prisms with a square cross-section of 500 μm × 500 μm from "big" HCP specimens [38]. Using this approach, small sized specimens with lower w/c ratios, e.g. 0.3 can be prepared, scanned and analysed [39].

To analyse the reconstructed microstructure quantitatively, an image thresholding procedure is required to segment the material into individual phases. Similar strategies used for BSE images are generally adopted. As shown in Fig. 7, because no discrete peak for the pore can be observed, the aforementioned tangent-slope method [25,40,41] or the "overflow" pore segmentation method [26] are generally used to determine the threshold between the pore and solid phases. An alternative approach is to fit the greyscale level histogram by multiple Gaussian through a deconvolu-
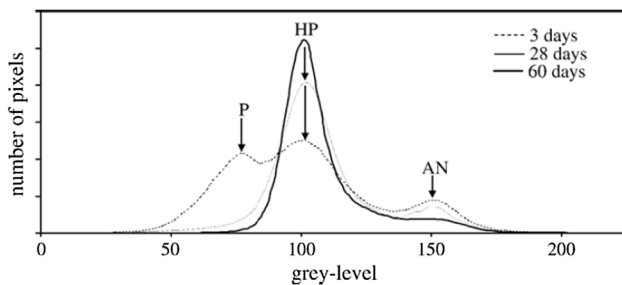
tion approach [42,43]. However, due to the limited resolution and the fact that hydration products such as C-S-H, CH, ettringite and monosulfate have a similar density, hydration products cannot be differentiated from the greyscale level histogram. As a consequence, they are generally considered together as a single phase [34,44–46]. An example of a segmented 3D material structure consisting of pore (P), hydration products (HP) and anhydrous cement grains (AN) is shown in Fig. 8, the tangent-slope approach [25] is used to isolate the pore from the solid matrix, while the tangent slope between HP and AN is considered as hydration products/anhydrous cement grains threshold value. Once the microstructure is available, a variety of computational tools exist to directly calculate the properties of the extracted digitalized microstructure, e.g. pore connectivity [35] and spatial distribution [34], transport [36,47] and mechanical [44] properties, based on which the microstructure - property relationships can be quantified.

2.2. Computer- generated material structure

A number of models have been proposed to simulate the hydration process of cement paste and thus offering its microstructure for further investigations. Comprehensive reviews of these models can be found in the literature [8,48–51]. The most important assumptions for these models involve the kinetics of hydration, initial particle packing and spatial distribution of products.

According to the adopted algorithm to describe the microstructure, two types of models can be distinguished: vector (also termed as continuum) and digital microstructural models. Commonly used models are summarized in Table 1. In vector models, particles are commonly stored as centroid and radii of shells. The hydration process is essentially simulated as particle growth with overlaps. On

Fig. 7. Greyscale level histograms of hardened cement paste at different curing time. From the right (highest grey levels) the peaks correspond to anhydrous cement particles, hydration products. The discrete peak for the porosity disappears with the hydration going on [5].

Table 1
Categories of main integrated kinetic cement hydration models [52].

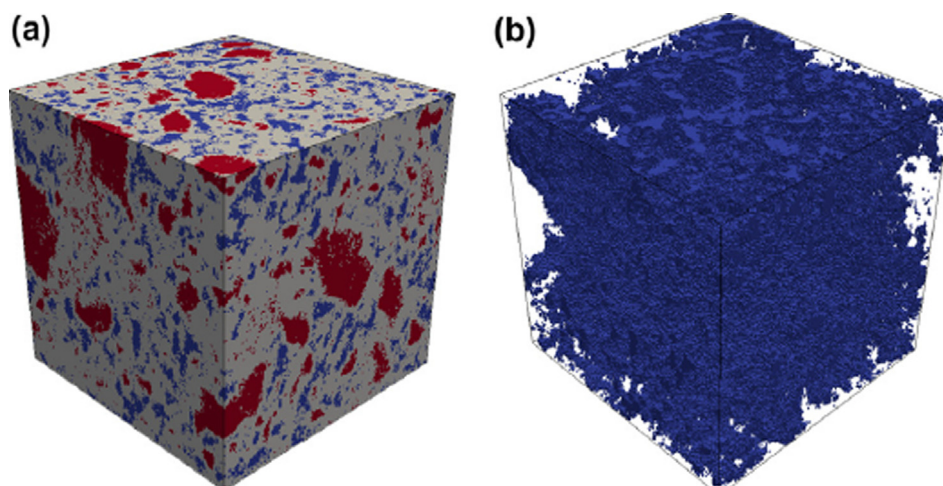| Categories	Names
Vector model	Model of Jennings and Johnson [53]
	HYMOSTRUC3D [6–8]
	Model of Navi and and Pignat [54]
	Model of Nothnagel and Budelmann [55]
	μic [9,10]
	Model of Wang et al. [56]
	Ducom [57]
Digital microstructural model	CEMHYD3D [11]
	HydraticCA [58]

Fig. 8. Spatial phase distribution obtained from μCT scanning and pore structure after thresholding (blue = pores; grey = hydration products; red = anhydrous cement grain) [36].

the other hand, digital microstructural models represent the microstructure using cubic voxels. Each voxel is occupied by a single phase (e.g. anhydrous cement particle, pore or a hydration product). The voxels can dissolve, diffuse and react to form new hydration phases.

2.2.1. Vector models

HYMOSTRUC3D and μic are the most widely used vector models. In HYMOSTRUC3D, the initial cement particle size is distributed on the basis of Rosin-Ramler distribution. The largest particle is placed in the centre of a representative volume. Other particles are packed around it and a periodic boundary is applied during the packing process. The hydration is controlled by the chemical composition and particle size distribution of the cement clinker, the water content and the temperature. With ongoing hydration, particles gradually dissolve and a porous shell of hydration products consisting of inner and outer hydration products forms around the particle. A 2D slice extracted from the simulated microstructure with size of $100 \times 100 \times 100 \ \mu m^3$ is shown in Fig. 9. The latest development of this model allows taking the deposition of CH into account [52]. Up to now, many mechanical performances, e.g. autogenous shrinkage [7], drying shrinkage [59] and fracture [60] of cement paste have been predicted on the basis of the microstructure obtained by HYMOSTRUC3D.

μic is another widely used numerical model for study of microstructure-property relationships of cement paste. It was developed by Bishnoi et al. [10] on the basis of work presented by Navi and Pignat [54]. In order to efficiently calculate overlap of spherical grains, several key algorithms involving grid subdivisions and point sampling are introduced in the model [9,10]. Fig. 10 shows a 2D slice from μic simulated 3D microstructure of cement paste. One of the advantages of this model is that it offers flexibility to set several parameters defining the reactions, which facilitates the understanding of the driving mechanisms of cement hydration. Elastic properties [61], creep and shrinkage behaviour [62] of cement paste have been predicted based on this model.

Although vector models are more computationally effective, the assumption of the spherical shapes of cement particles has a significant effect on the simulated hydration progress [64]. Furthermore, it is reported that the assumed morphology of hydrates in the simulated microstructure significantly influences micromechanics-based elastic stiffness estimates of cement paste, particularly at very early age [65].

Fig. 10. A 2D slice from 3D microstructure of cement paste simulated by μic platform [63] (red = anhydrous cement particles; blue = C-S-H; green = CH; black = pores).
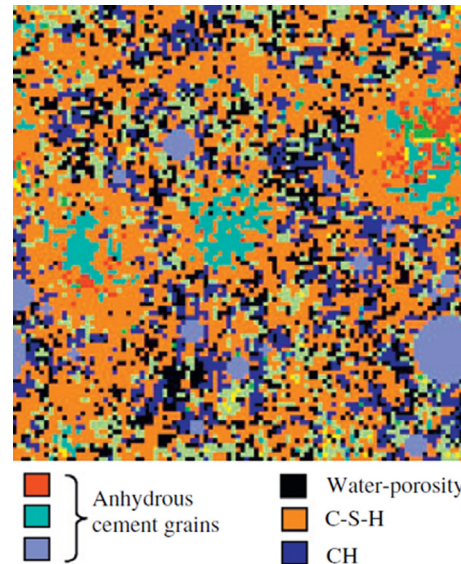
Fig. 11. A 2D slice from 3D microstructure of cement paste simulated by CEMHYD3D after [72].

2.2.2. Digital models

CEMHYD3D [11] is the most used digital microstructural model in cement science. It permits a direct representation of multiphase, multi-size and non-spherical cement particles using SEM images (see Fig. 11). In the current version, irregular particles are generated on the basis of the results from X-Ray tomography [66]. As the output from the model is already in a discretized form, finite element approach can be easily applied to calculate its mechanical properties [46,67-69]. This approach is simple and effective in terms of application for finite element modelling of mechanical properties [9]. However, time scale in the model is not defined as the physical time because of the cellular-automata scheme [70] used for the hydration simulation. Essential calibrations are therefore required [51]. To overcome the aforementioned limitations, a new model named HydratiCA has recently been proposed on the basis of more fundamental principles of reaction kinetics and thermodynamics [58,71]. Although a lot can be expected from this model, it is still under development.
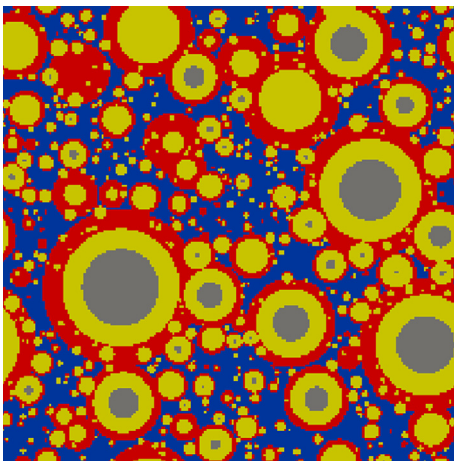
Fig. 9. A 2D slice from 3D microstructure of cement paste simulated by HYMOSTRUC3D (grey = anhydrous cement particles; yellow = inner hydration products; red = outer hydration products; blue = pores).
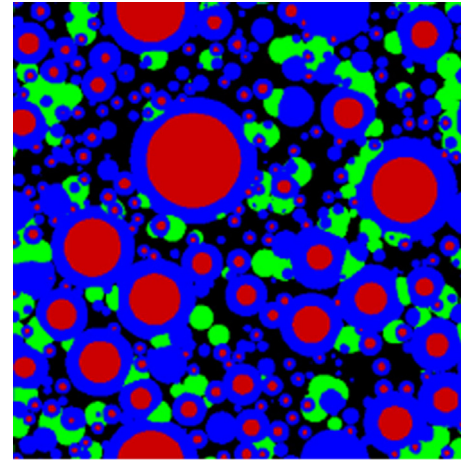
3. Mechanical properties characterization of individual phases

3.1. Nanoindentation technique

Nanoindentation has become a general tool for assessment of micromechanical properties, i.e. elastic modulus and hardness of individual constituents, of hardened cement paste. As such, it is commonly used for providing input for micromechanical models. This section reviews its principles, testing strategies and newly developed test configurations for the strength properties measurements.

3.1.1. Principle

The basic idea of nanoindentation is simple: push a very sharp hard tip with known geometry and mechanical properties into the surface of a material and investigate the bulk elastic behaviour of the material from the recorded load–displacement curve. For this purpose, a three sided pyramid Berkovich tip is commonly used. A typical load–displacement curve and the deformation pattern of an elastic - plastic sample during and after indentation are shown in Fig. 12. The indenter is first pressed into a flat surface under a constant loading rate. To avoid plastic effects, the indenter is held for a few seconds at the prescribed maximum load (indentation depth), after which the specimen is unloaded. This allows a direct measurement of the hardness and the elastic modulus using the method proposed by Oliver and Pharr [73] on the basis of analytical solutions applicable to homogeneous and isotropic half-space with a flat surface. The hardness H can be obtained at the peak load as:

$$H = \left(\frac{P}{A}\right)\Bigg|_{h=h_{max}} \tag{2}$$

where h is the displacement relative to the initial surface, A the projected area which is a function of the function of the contact depth h_c for an indenter tip with a known geometry. In terms of assessment of the elastic modulus, it is assumed that during the unloading phase only elastic displacements are recovered and that the reduced elastic modulus, also known as indentation modulus M, can be determined using the slope of the unloading curve:

$$S = \left(\frac{dP}{dh}\right)\Bigg|_{h=h_{max}} = \frac{2}{\sqrt{\pi}} M \sqrt{A} \tag{3}$$

where S is the elastic unloading stiffness defined as the slope of the upper portion of the unloading curve during the initial stages of unloading. As M accounts for the deformation which occurs in both the indented material and the indenter, a correction is made following Hertz's contact solution [74]:

$$M = \frac{1 - v_s^2}{E_s} + \frac{1 - v_i^2}{E_i} \tag{4}$$

where v_i and E_i refer to indenter's Poisson's ratio and Young's modulus (0.07 and 1140 GPa, respectively, for a diamond indenter), and v_s, E_s are the corresponding properties for the tested material.

3.1.2. Nanoindentation of hydrated cement paste

As mentioned above, nanoindentation is designed for assessing mechanical properties of homogenous materials, e.g. ceramics [76] and glass [77]. In terms of heterogeneous materials, like cement paste, the nanoindentation measurements encompass mechanical properties of the local (indented) material microstructure but also the microstructure around the indent (generally termed the interaction volume [78]) with the length scale around 3–5 h_{max} [79,80].

In order to derive the mechanical properties of individual constituents in cement paste, several strategies have been developed. Basically, two strategies can be summarized in terms of whether additional instruments are required.

The first one is the so-called statistical nano-indentation. It is based on a combination of grid indentation and deconvolution approach with no need of known details (e.g. chemical compositions, phase deification) of the indented location for each indentation. As schematically shown in Fig. 13, a large number of indents ($\geq$400, in general) are performed on the matrix surface. According to the scale separation theory, when the grid size and indentation depth are chosen properly (a general rule-of-thumb is that $h_{max} \leq D/10$, where D is the characteristic size of the phases [81,82]), each indentation test may be treated as an independent statistical event, and a subsequent statistical deconvolution of the indentation results can be applied. Briefly, the deconvolution approach involves fitting n Gaussian distributions to the experimental probability density function (PDF, see Fig. 14) or cumulative distribution function (CDF, see Fig. 15) and generating the theoretical PDF for the grid nanoindentation data. More details about the deconvolution approach can be found in [75,81] for the PDF and in [83,84] for fitting the CDF. Furthermore, it is worth mentioning that, because generation of the experimental PDF requires a choice of bin-size for histogram construction, it is analytically more convenient to deconvolute the CDF rather than the PDF [83,84]. However, it should be noted that the scatter in the resulting mechanical properties of individual cement phases is high and it is debated in literature whether this method can be used at all for heterogeneous materials like cement paste [85–89]. A reason for this is that, although the tip-radius is very small (in case of the typically used Berkovich tip), it is almost impossible to probe a single phase; in fact, a composite made up of different phases is probed by indenting the material with a diamond tip [85].
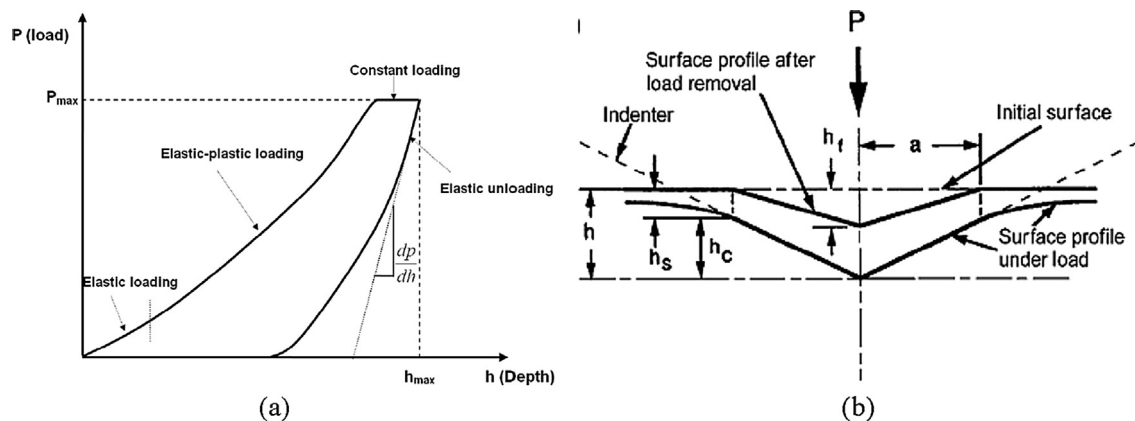

Fig. 12. (a) A typical load–displacement curve [75] and (b) the deformation pattern of an elastic - plastic sample during and after indentation [73].
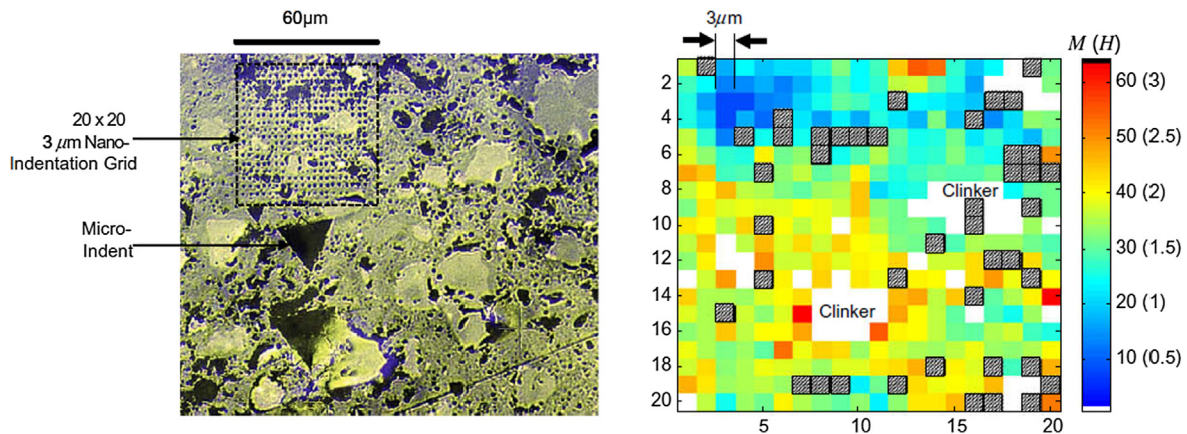
Fig. 13. A schematic view of grid indentation technique applied on cement paste (left) and maps of the derived mechanical properties of the test area [87].
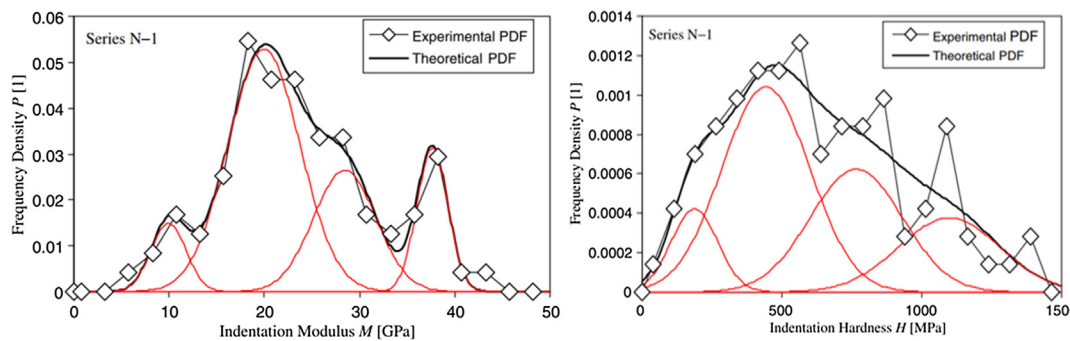

Fig. 14. Example of statistical deconvolution of PDF after [81].
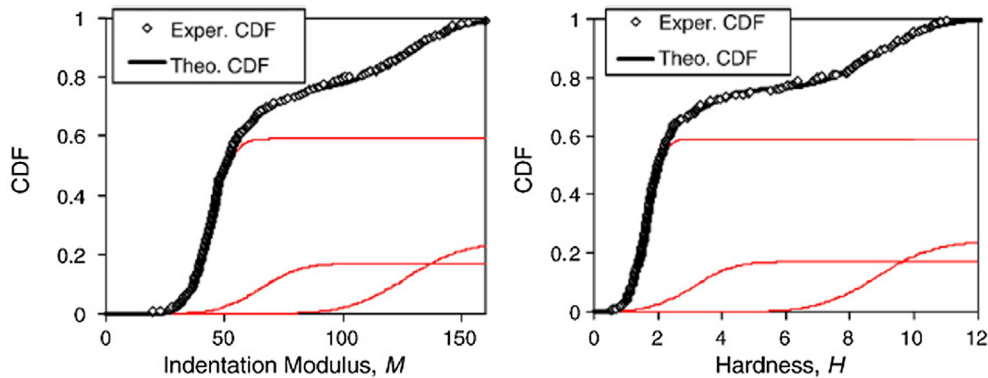
Fig. 15. Example of statistical deconvolution of CDF after [84].

The second strategy relies on the knowledge about the indented microstructure with aid of the SEM. In this strategy, the indents are performed to a material phase with indentation depth smaller than the characteristic dimension of the tested phase. As shown in Fig. 16, SEM is adopted to visualize and characterize the microstructures where nanoindentation tests were performed under the BSE mode. The intrinsic properties of these indistinct phases (still intrinsic phase porosity underneath h cannot be excluded) can be obtained separately. However, it should be noticed that when dealing with cement paste, which is a 3D heterogeneous material, the indentation outcome is always influenced by the underlying material, which can be stiffer and harder than the indented phase or vice versa [89]. A possibility to determine whether the local indentation response was a result of a single- or a multiphase response, is to couple the grid-indentation with ex situ scanning electron microscope-energy-dispersive X-ray (SEM-EDS) [80]. As shown in Fig. 17, by properly choosing the indentation depth and set up of EDS (accelerating voltage, beam current and working distance), the interaction volumes probed by both methods is of a comparable size. The mechanical information provided by nanoindentation can be therefore directly correlated with the chemical information provided by SEM-EDS (Fig. 18).

Using the grid indentation technique, elastic properties of clinker phases, e.g. C_3S, C_2S, C_3A and C_4AF have been tested and reported in [90]. With respect to C-S-H, numerous indentation tests have been conducted. A comprehensive review can be found in [75]. For the low-density C-S-H, the average indentation
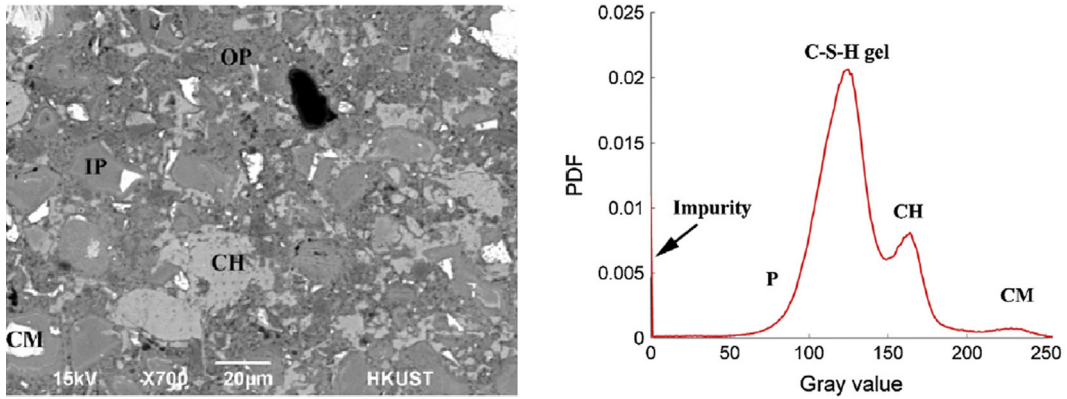
Fig. 16. BSE image of the indented area to identify the microstructure structure information of each indent (left) by using the image segmentation on the right side [12].
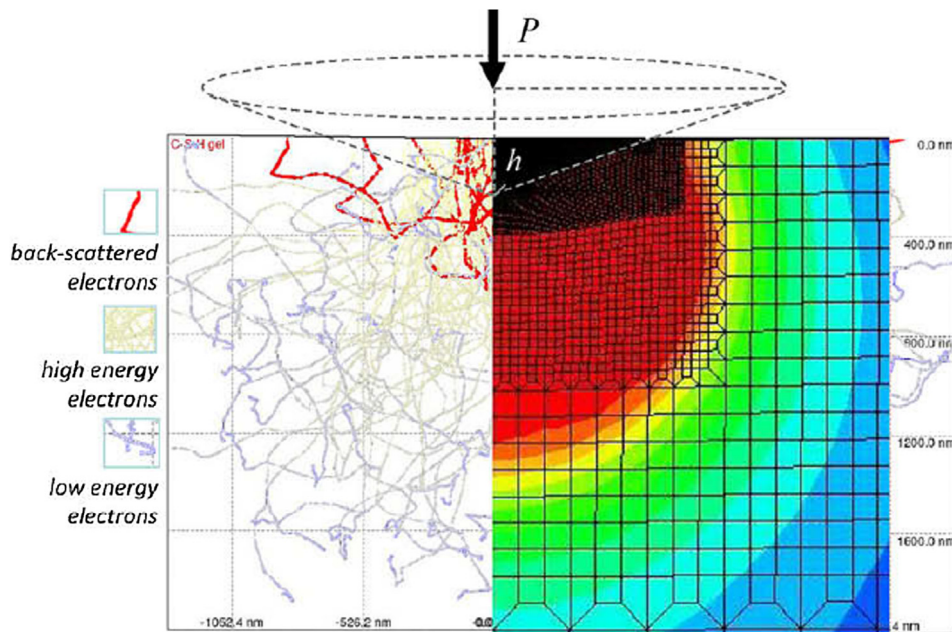
Fig. 17. Interaction volumes probed respectively chemically by Wavelength Dispersive Spectroscopy and mechanically by nanoindentation (right): the left-half of the figure displays results of Monte Carlo simulation of electron beam penetration of C–S–H gel. The right-half represents finite element results of Von-Mises stresses below the indenter, after [87].
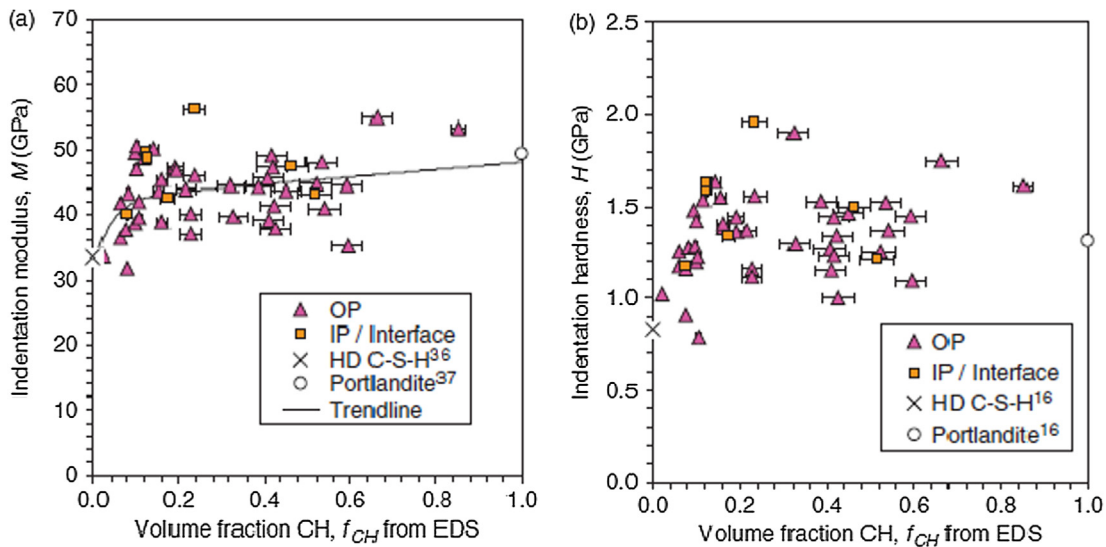
Fig. 18. (a) Indentation modulus M and (b) indentation hardness H plotted as a function of the volume fraction of CH in micro-volumes containing CH and C-S-H [80].

modulus varies from 18.1 to 26.84 GPa, while a range between 29.1 and 36.1 GPa is found for the high-density C-S-H [13,14,81,91–94]. Note that these reported properties include the effect of porosity and embedded monocrystalline CH or minor compounds present at smaller scales. The other hydration product e.g., CH has been characterised as 38 ± 5 GPa, which is similar to the high density C-S-H [13].

3.2. Universal testing using nanoindenter

While nanoindentation may be considered appropriate for measuring the elastic properties of cement paste and its individual phases, more complex procedures are needed for measuring strength properties at the micrometre length scale.

Recently, use of a nanoindenter has been proposed by several researchers to measure the tensile strength of cement paste [95] and individual hydration phases [27] using micro-cantilever bending tests. This technique consists of specimen preparation using a focused Ga$^+$-ion beam milling. With this procedure, micro-cantilevers with a triangular (Fig. 19) or rectangular cross-section (Fig. 20) can be created by milling the solid matrix. Typically, the length of these micro-cantilevers is up to 10 μm. These cantilevers are subsequently subjected to bending by applying a load at the end of the cantilever using the nanoindenter or an atomic force microscope. This provides a measure of the elastic modulus and the flexural strength of the micro-volume. Similarly, a micro-pillar compression technique involving focused ion milling of a
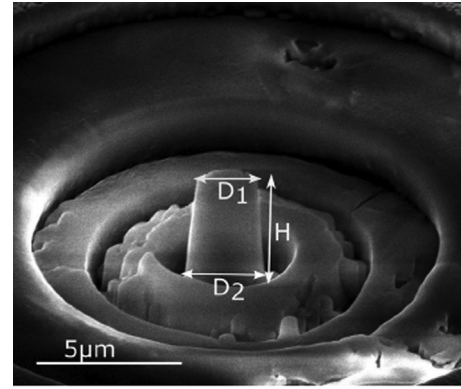

Fig. 21. SEM image of a micro-pillar after [96].

micro-pillar in the material (Fig. 21) and a compression test using the nanoindenter has been performed by Shahrin and Bobko [96,97] to measure the compressive strength and modulus of the C-S-H particles in the cement paste matrix. However, a major drawback of this approach is the time-consuming specimen preparation. Consequently, a relatively small number of specimens can be prepared and analysed [97,98]. At small (i.e., micrometre) length scales, a high scatter of measured mechanical properties is expected [99]. Therefore, a large number of tests need to be performed for the measurements to be statistically reliable. Furthermore, as reported by Němeček et al. [100], both the FIB milling introduced local heating and the vacuum environment inside the electron microscope chamber have significant influence on the microstructure of the prepared specimens. Therefore, low energy milling should be used for the sample preparation and high vacuum should be avoided during the mechanical test.

3.3. Atomistic simulations

An alternative way to derive the mechanical properties of individual phases present in the cementitious materials is by using atomistic simulations, e.g. ab-initio, Monte Carlo and Molecular Dynamics, etc. On the basis of these techniques, the elastic response of the crystalline phases has been analysed. Dolado and van Breguel [50] compared these computed elastic properties with the experimental measurements reported in the literature. In terms of the clinker phases, a good agreement can be found for C$_3$S [101,102], C$_2$S [101,102] and C$_3$A [101–103], while a big dispersion occurs for C$_4$AF. No clear explanation is available for this disagreement. With respect to the crystalline hydrates, the atomistic simulations reproduce well the experimental values of CH (35–48 GPa) [101],
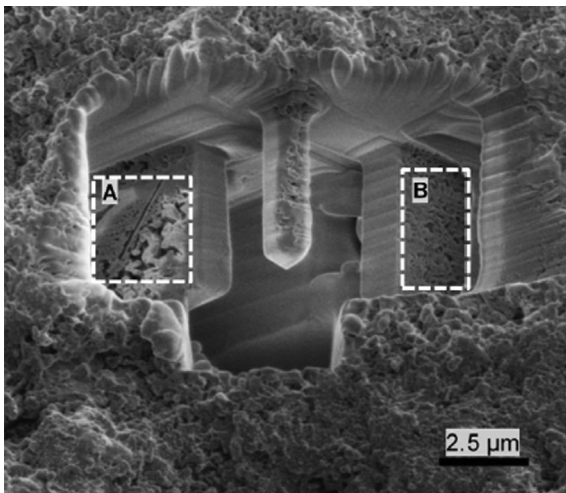

Fig. 19. ESEM image of the micro-cantilever with a rectangular cross-section after [95].

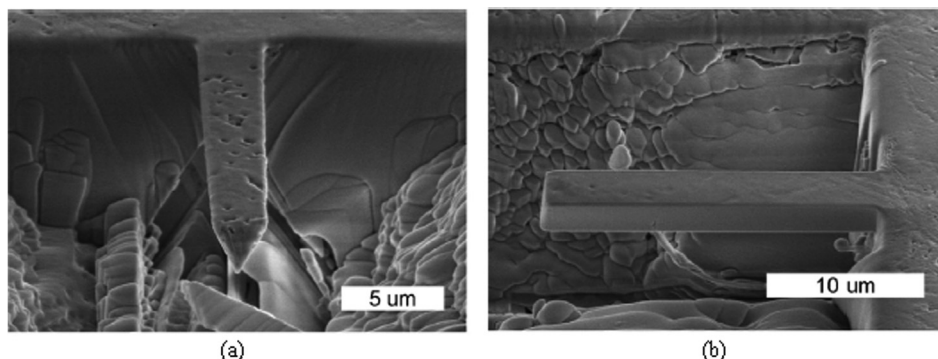**Fig. 20.** ESEM image of the micro-cantilever with a triangular cross-section after [27]: (a) front view; (b) side view.

while the complex structure of ettringite introduces a mismatch between the simulation and measurement [101,104].

The real challenge for atomistic simulations is the description of the C-S-H gel. This is due to its amorphous structure and the lack of direct observations at the atomistic level. Thus, much of the actual knowledge on the C-S-H gel is derived on the basis of simulations of its mineral analogues (tobermorite and jennite) or different morphological features presented in both layered models [105–110]. Prediction of the elastic properties of these crystalline minerals can be found in [16,101,110,111]. On the basis of some basic characteristics of the C-S-H gel measured by nanoscale techniques, a "realistic C-S-H model" has been proposed by Pellenq *et al.* [17] using Molecular Dynamic and the Grand Canonical Monte Carlo (Fig. 22). The predicted anisotropic Young's modulus (55 GPa along y direction, 66–68 GPa along the x-z plane) is in accordance with the value derived by nanoindention (65 GPa) [81]. On the basis of the presented C-S-H model, the tensile strength of the atomistic structure is estimated to be between 1 and 3 GPa depending on the relative humidity. Hou *et al.* [112] implemented a uniaxial tensile test on this model to study the influence of the size of gel voids on the fracture response of a 138 Å × 138 Å × 138 Å C-S-H unit, see Fig. 23. In their study, a significant decrease in terms of the stiffness and strength is observed
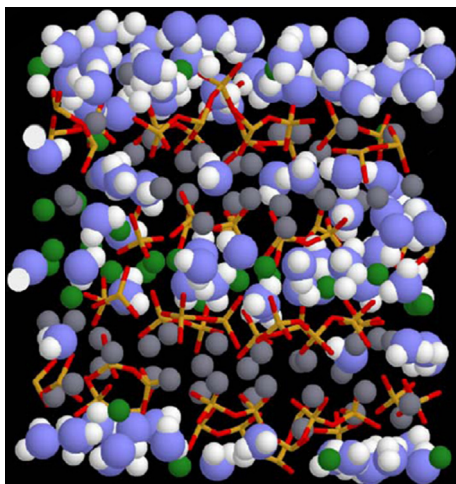

Fig. 22. A molecular model of C-S-H from [17]: the blue and white spheres are oxygen and hydrogen atoms of water molecules, respectively; the green and grey spheres are inter and intra-layer calcium ions, respectively; yellow and red sticks are silicon and oxygen atoms in silica tetrahedral.
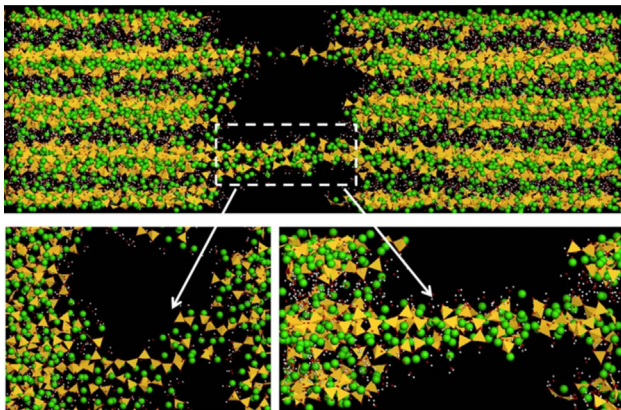

Fig. 23. Fracture configuration of C-S-H gel after the uniaxial tension test after [112]: yellow tetrahedron represents silicate tetrahedron; green balls represent calcium atoms and white points are water molecules.

due to the presence of the gel pores. This indicates that the gel porosity at the nano-scale is detrimental to the mechanical properties of the C-S-H gel.

To better understand the properties of the cement hydrate with complex structure and various compositions, Hou *et al.* [113-115] further developed a series of atomistic models of the C-S-H gel. Their study found that the mechanical properties of the C-S-H gel is greatly dependent on the chemical composition. Both the stiffness and the cohesive force of the C − S − H gel are weakened by breakage of silicate chains and penetration of water molecules with increasing of Ca/Si ratio and H_2O content [116]. In their study, the reactive force field also allows the chemical reactions of the C-S-H gel subjected to external loading. The molecular study can provide a scientific guideline for the design of cement-based materials at the nanoscale and improve the mechanical weakness of the cement-based material such as low tensile strength and quasi-brittle fracture behaviour.

Although atomistic simulations are promising, this is still a new field of research in terms of cementitious materials. Furthermore, due to the current computational capacities, atomistic simulations can only be performed on a very small piece of material (up to 10 nm) [50]. In a typical micromechanical model, the resolution is generally around 0.5–2.0 μm. As a consequence, a scale gap between the micro- and the nano-scales is present and cannot be bridged by the atomistic simulation only. Thus, an intermediate level, termed as the sub-micro level, has been proposed to computationally describe C-S-H gel on the scale ranging from tens to hundreds of nanometres. At this scale, the high-density and low-density C-S-H can be assembled by these small C-S-H bricks obtained from the nano-scale on the basis of a packing factor [117,118]. Although several pioneering works have been done [119–123], additional research is required in the development of relations bridging the nano- and the micro-scale [124].

4. Micromechanical modelling

4.1. Effective mechanical properties

Based on the assumptions of the existence of a representative volume element (RVE), homogenization techniques derive the definitive effective properties of a heterogonous material by "averaging" the detailed fields in the RVE. Specifically, for the known stress field σ_{ij} and strain field ε_{ij} under certain applied load, the averaged stresses $\bar{\sigma}_{ij}$ and strains $\bar{\varepsilon}_{ij}$ over the RVE are normally defined as [125]:

$$\bar{\sigma}_{ij} = \frac{1}{V} \int_V \sigma_{ij} dV \tag{5}$$

$$\bar{\varepsilon}_{ij} = \frac{1}{V} \int_V \varepsilon_{ij} dV \tag{6}$$

where V is the volume of the RVE. When linear elasticity is assumed, Hooke's law can be applied as:

$$\bar{\sigma}_{ij} = C_{ijkl} \bar{\varepsilon}_{kl} \tag{7}$$

Here C_{ijkl} is defined as the effective stiffness tensor for the homogenized heterogonous material structure. Thus, in order to calculate the homogenized properties of a material, the exact solutions of the stress and strain fields at each point are needed. To obtain these exact solutions, several techniques have been proposed. These techniques can be divided into two categories: analytical and numerical.

Analytical approaches require idealized geometric models. Mori-Tanaka [126] and Self-Consistent [127] are the commonly used schemes to link the composite geometrical structure with its effective properties at the micro-scale. The basic assumptions
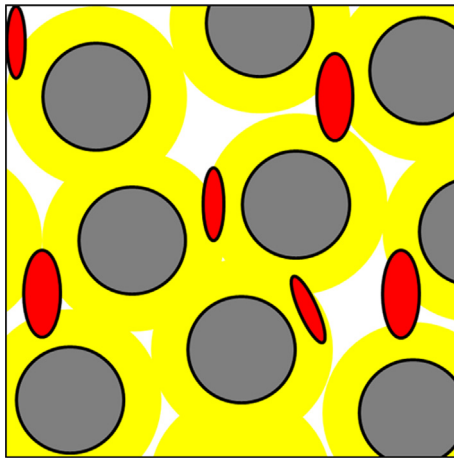
Fig. 24. Polycrystalline RVE of "cement paste" built up of C-S-H, aluminates, anhydrous cement particles and capillary pores (modelled by Self-Consistent scheme, the image has been reformed for clarity), after [13].

Fig. 26. Comparison of predicted Young's modulus with experimental results (error bars indicate standard deviation) [41].

in these two schemes are matrix-inclusion morphology and mechanical interactions between particles. As shown in Fig. 24, at the micro-scale, cement paste matrix is represented by the C-S-H matrix, together with anhydrous cement products, large CH crystals, aluminates, and capillary pores. Since they are largely disordered and in contact with each other, Self-Consistent scheme is generally used. However, this approach cannot deal with the clustered structures or microstructures with large differences between properties of the phases. When big difference occurs in the stiffness between matrix and inclusions (see Fig. 25), the Mori-Tanaka approach should be adopted to consider the mechanical interactions between inclusions [13,128]. Due to its high computational efficiency, the application of analytical homogenization is mainly focused on the predicting the evolution of elastic properties of cementitious materials [65,67,128,129]. The influence of the shape of the individual phases on the predicted effective elastic properties has been reported in [65,129]. Furthermore, the compressive strength of cement paste can be estimated by calculating the deviatoric stress peak from the elastic energy stored in the RVE [65,130,131]. Furthermore, it is worth mentioning that there are other homogenization techniques, e.g. differential scheme [132] and direct particles interaction method [133]. While promising in certain aspects, relatively few studies on micromechanical properties of HCP have been carried out using these schemes so far.

As mentioned above, analytical approaches are only applicable for idealised material microstructures. When dealing with more realistic and complex material structure as mentioned in **Section 2**,
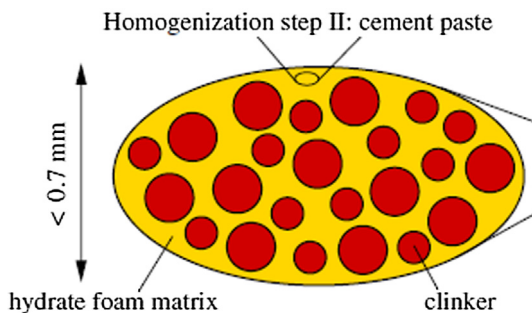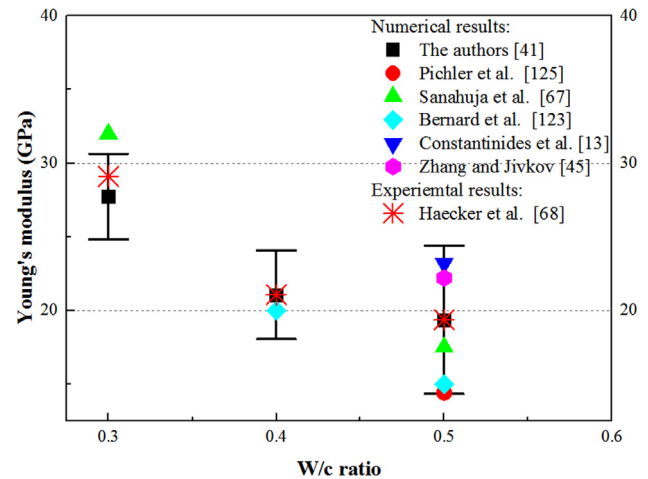
numerical approaches have to be used. The finite element method (FEM) has been extensively used to analyse the elastic properties of complex microstructure of cement paste obtained from CEM-HYD3D [68,134], μCT [46,135] and μic [61] through the homogenization technique. As an alternative to FEM, Fast Fourier Transform (FFT) has been adopted by Šmilauer and Bittnar to model the evolution of elastic properties of the hydrating cement paste [136]. A comparison between analytical and numerical approaches seems to favour the utilization of FEM for microstructure at early ages where higher porosity exists. Stora et al. [137] concluded that when capillary porosity is above 35%, the analytical schemes fail to account for the interactions between inclusions. Although comparable results were found for the numerical and analytical schemes for sound hydrated paste where spherical and prismatic inclusions exist in the matrix [138], the volume fraction of inclusion should not exceed 30% when the Mori-Tanaka approach is used.

The authors [41] have compared the simulated Young's modulus of HCPs with various w/c ratios (0.3, 0.4 and 0.5) in the literature using different approaches. Clearly, as shown in Fig. 26, dispersion occurs. This is mainly because of the heterogeneous nature of such materials. The authors used 10 cubic digital samples for each w/c ratio obtained from μCT to calculate the elastic modulus, the average value and standard deviation are shown in Fig. 26. In terms of simulating results of HCP with w/c ratios 0.5 and 0.4, data from literature all falls into the intervals, while this does not apply for w/c ratio 0.3. However, as shown in Ref. [41], there is one sample having the similar elastic Young's modulus with Ref [67]. Therefore, it is recommended to study HCPs in a stochastic way.

4.2. Stress–strain response

As the failure of cementitious materials at the meso- or macro-scale is mostly governed by the local tensile stress, the fracture behaviour of cement paste under uniaxial tension is very important. One of the most important outputs from such computational uniaxial tension modelling is the stress–strain response. The tensile strength, elastic modulus and fracture energy can be derived from this response. Bernard et al. [139] incorporated the digitalized microstructure from CEMHYD3D in a finite element software Abaqus as input for a fracture analysis. In their work, 3D solid linear finite elements are used. A Rankine criterion is adopted to model the failure of the different phases. Zhang and Jivkov [44,45] applied a site-bond model to predict the micromechanical properties of

Fig. 25. RVE of matrix-inclusion composite "cement paste" where a spherical clinker phase is embedded in a hydrate foam matrix (modelled by Mori–Tanaka scheme), after [130].
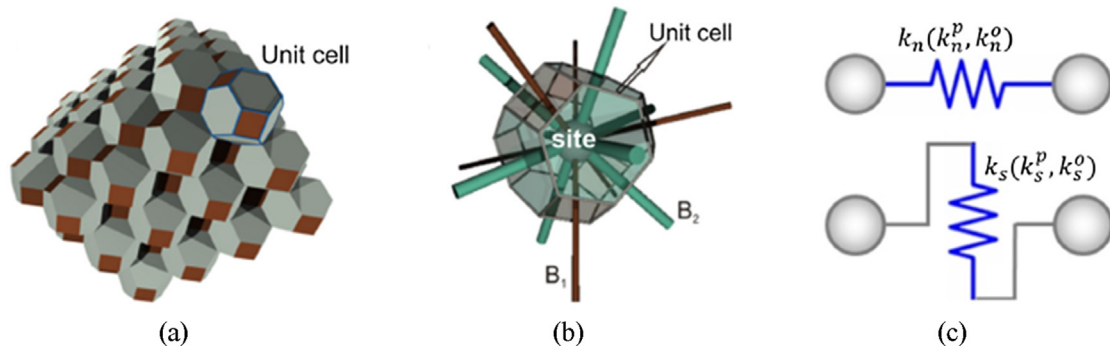
Fig. 27. Schematic view of a site-bond model: (a) site-bond assembly; (b) unit cell with bonds; (c) normal and shear springs [44,45].
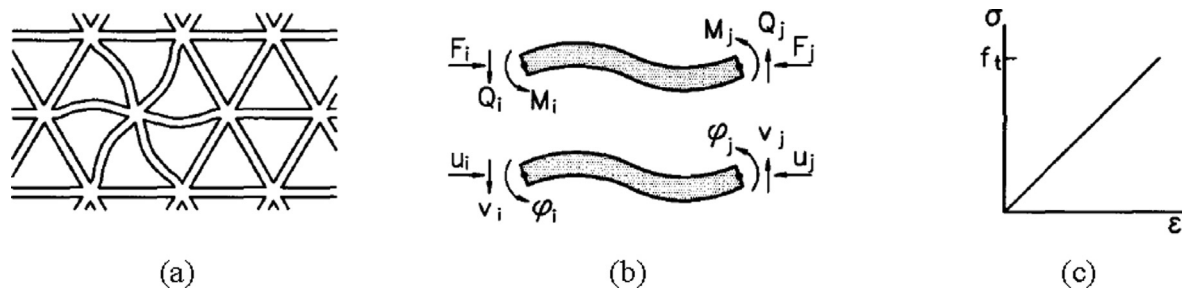

Fig. 28. Schematic view of a discrete lattice model in 2D: (a) regular triangular lattice of beams; (b) external forces and deformations on a single beam element (c); pure elastic constitutive law for an element [140].

cement paste. In the site-bond model, the material volume is represented by an assembly of truncated octahedral cells, each of which consists of six square and eight regular hexagonal faces, as shown in Fig. 27. A homogenization approach is applied to obtain the mechanical parameters of each cell on the basis of the features, i.e. size distribution of anhydrous particles and capillary pores obtained from the segmented μCT images. An energy-based failure criterion is used to determine the failure of the bond between two cells. The fracture process is modelled by continuously increasing the strain and removing the failed bond until the prescribed strain is reached. Similar like the site-bond model, discrete lattice model [140] discretises the material volume as a set of beam elements with linear elastic behaviour, see Fig. 28. The crack growth is simulated by using a sequentially-linear solution procedure [141]. This procedure involves performing a linear elastic analysis in every step; then, a single element with the highest stress/strength ratio is identified and removed from the mesh, thereby introducing a discontinuity; this procedure is then repeated until a global failure criterion is reached. On the basis of such model, the fracture process of micro cement paste cubes under uniaxial tension has been reported by Qian [60] and Luković *et al.* [89] respectively. Recently, a crack phase field model has been utilized by Han *et al.* [34] to analyse the μCT generated material structure. Such model requires Young's modulus and Poisson's ratio for the solid phase and two key modelling parameters for material degradation, namely the fracture energy and the diffusive length parameter.

The simulated stress–strain curves of the aforementioned works are compared in Fig. 29. Although comparable results are found for the stiffness, a large difference in terms of the strength (peak stress) is observed for these models. This is mainly because the elastic properties of each phase they considered in the model are more or less the same (typically taken from nanoindention measurements), while other parameters that govern the crack development are difficult to determine due to lack of experimental measurements at the small length scale. The result from Bernard

et al. [139] shows the lowest strength. This mostly attributed to the fact that the tensile strength of each phase is assumed as 1/1000 of its elastic modulus in the model. Although this ratio is in accordance with the phenomena observed at the macro-scale, it has been shown in [27,142,143] that this ratio increases with the observed scale decreasing. Luković *et al.* assumed [89] the tensile strength as 1/30 of the material hardness measured from nanoindentation, resulting in a much higher simulated tensile strength. Han *et al.* [34] used the modelling results from [89] to calibrate their model. This is the reason why comparable strengths are obtained for [89] and [34]. Although identical model and material structure features were used by Zhang and Jivkov [44,45], the predicted strength from their earlier work [44] is much higher compared with the latter [45]. This is because different approaches are applied to homogenise the mechanical properties of each cell. Such homogenization procedure would also decrease the heterogeneity that could be explicitly present in the model. This leads to a much more brittle post-peak behaviour compared with the results reported in [60,89] in which similar strategy is implemented for the crack development. Furthermore, it is worth mentioning that, although the same fracture model is applied, different elastic properties were obtained by Qian [60] and Luković *et al.* [89] due to different material heterogeneities that have been implemented. Qian [60] used the microstructure obtained from HYMOSTRUC3D. On the other hand, Luković *et al.* [89] overlapped the spatial distribution of mechanical properties from grid nanoindention measurements directly to the lattice network. In this approach, defects larger than the interaction volume of indentation test cannot be considered. Consequentially, the lattice system in Luković *et al.* [89] is stiffer than the one reported by Qian [60]. Thus, the approach to consider the original heterogeneity into the discrete model also plays an important role on the predicted mechanical performance. An alternative approach is to apply the heterogeneity using original greyscale images obtained by μCT [144,145], see Fig. 30. As reported by the authors, a strong linear
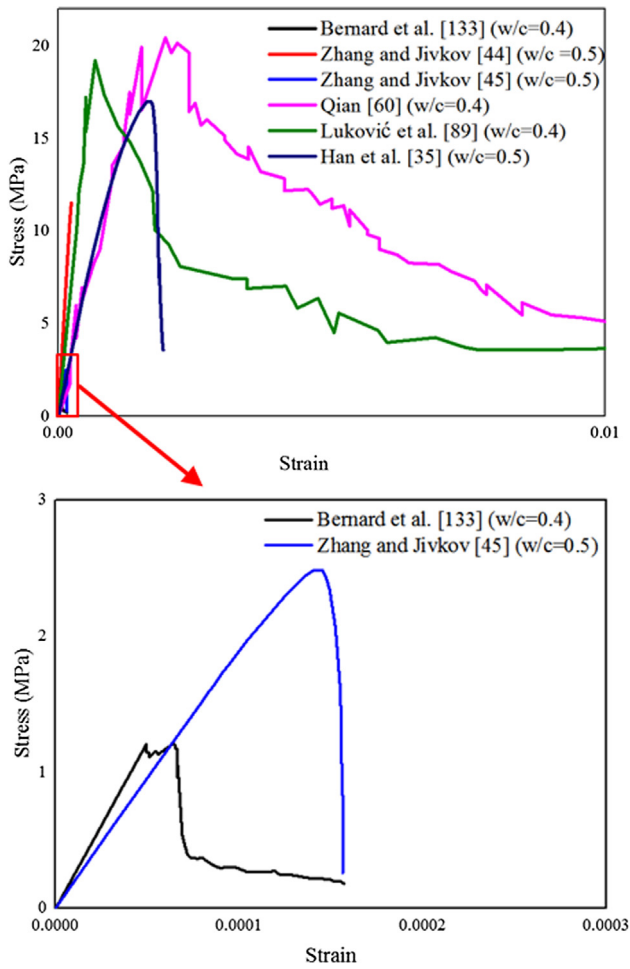
Fig. 29. Comparison of the simulated stress–strain responses of cement paste under uniaxial tension in the literature.

correlation between the greyscale level and indentation modulus is found. A linear equation is therefore used to link these two parameters. This approach is more generic and direct, as no processing of the μCT images (image segmentation) and the measured micromechanical properties (deconvolution) is required. A similar approach has been proposed by Monfared et al. [146] for correlating the nanoindentation measurements and μCT of organic-rich shales.

It is therefore important to note that, apart from the material structure, the predicted mechanical properties strongly depend on the assigned value of each model parameters. As the predicted

results are going to be up-scaled for the models at meso- or even macro-scale, it is essential to validate these results at the micro-scale. Therefore, mechanical tests at the micro-scale are highly desired to be conducted to calibrate the input parameters for the models.

5. Calibration and validation

Due to complex multi-scale heterogeneous material structure [147,148] and size effect [149–151], the calibration of the model-parameters and validation of the micromechanical models are possible when an experiment on the same size specimen is available. However, mechanical testing of cementitious materials at the micro-scale has long been recognized as a challenging task. Micro-scale sized HCP specimens cannot be cast in the small sized mode due to the surface tension of water nor measured by any conventional laboratory test method. Therefore, there is an essential need of developing advanced techniques for preparation and mechanical measurements of the micro-scale sized specimens.

There are some preliminary works can be found in the literature. Micro-scale sized specimens can be produced by thin-sectioning and micro-dicing using a micro-dicing saw [38]. Fig. 31 shows the cutting procedure and fabricated ESEM micrographs of 100 μm HCP micro-cubes on the glass substrate. The nanoindenter was used to load these produced specimens and measure the displacement-load response. Different indenter tips have been used to apply various loadings, see Fig. 32. The pyramid Berkovich tip was used to rupture the micro-cube, see Fig. 32a [38]. The observed typical failure mechanism is the splitting of the material under the tip and three main cracks running to the sides of the cubes, starting from the three edges of the Berkovich tip. As shown in Fig. 32b, one-sided splitting test can be conducted using a wedge tip to apply the load across the middle axis, which results in the micro-cube splitting in half [152]. Another test performed is the micro-cube compression test, in which a flat end tip is used to apply the compressive force on the top surface of the specimen [153]. Discrete lattice-type fracture model, using microstructural information obtained by X-ray computed tomography as input, was used to model the fracture process of the tested micro-cubes. The experimental measured load–displacement responses and observed fracture patterns can therefore be used to calibrate and validate the modelling results. After calibration and validation, the models can be used to predict the response of 100 μm cubes under idealised loading conditions, e.g. uniaxial tension and compression, see Fig. 33. A ratio of compressive/tensile strength ranges from 7.91 to 9.66 is found, which is in accordance with commonly reported values for concrete on the meso and macro-scale [154]. These modelling and testing techniques were further developed
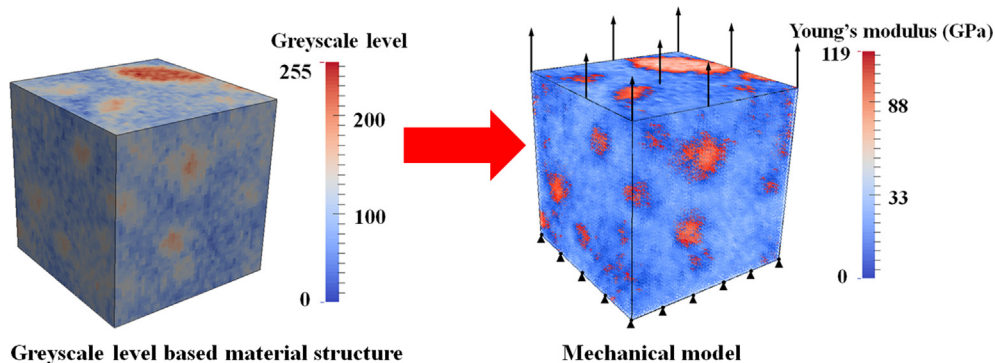
Fig. 30. Mapping of elastic properties on the basis of the greyscale level based material structure, after [144].

(a)

(b)
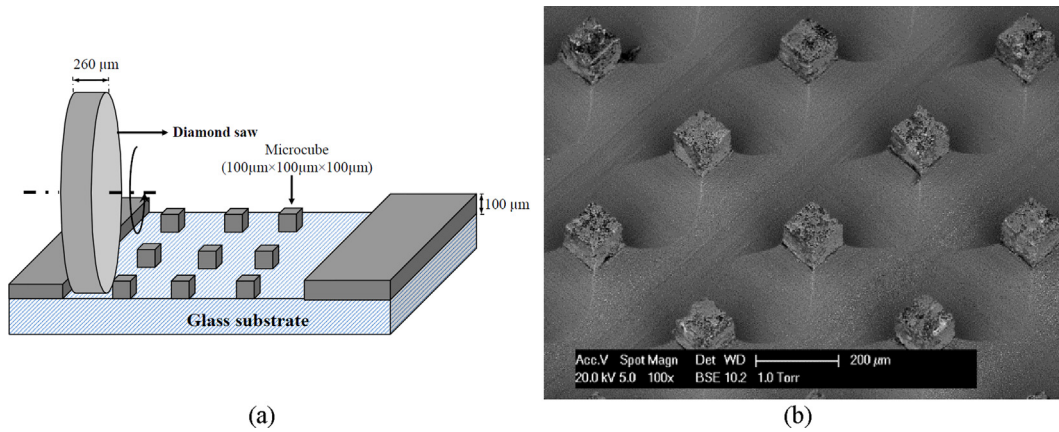
Fig. 31. (a) Schematic view of HCP micro-cube preparation; (b) ESEM micrographs of produced HCP micro-cubes after [38,149].

(a)

(b)

(c)
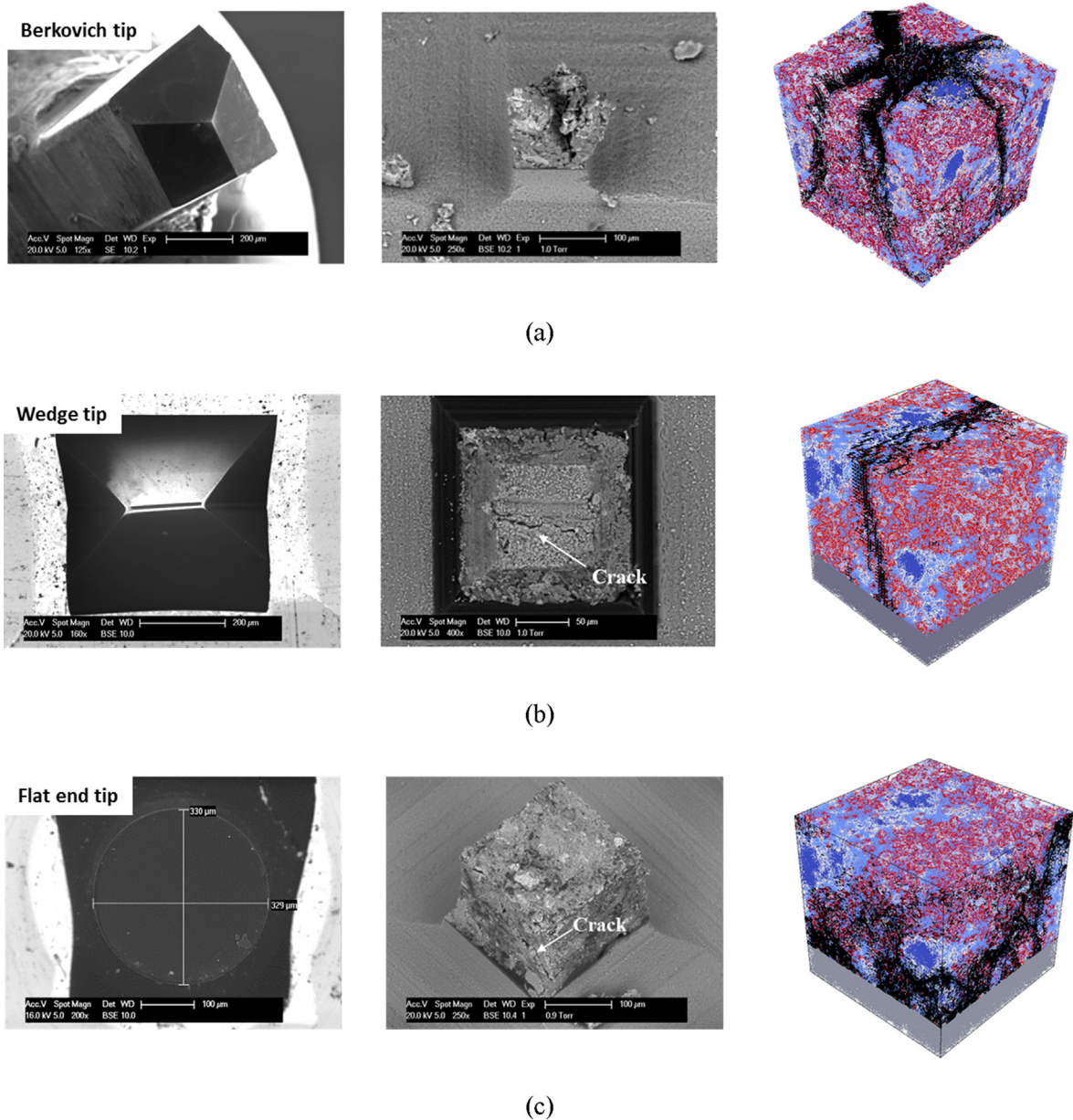
Fig. 32. (a) Schematic view of micro-cube indentation test which was used for the calibration of the micromechanical model [38]. (b) Schematic view of micro-cube one-sided splitting test which was used for the validation of the micromechanical model [158]. (c) Schematic view of micro-cube compression test which was used for the validation of the micromechanical model [153].
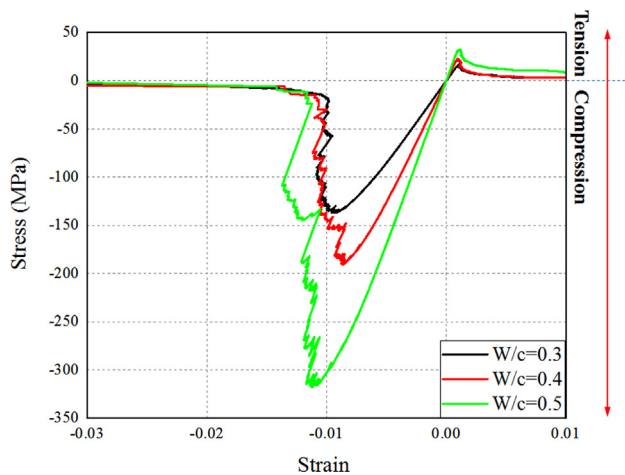
Fig. 33. Simulated stress–strain curves of 100 μm HCP cubes with various w/c ratios under uniaxial tension and compression.

by the authors to predict the micromechanical properties of the interfacial transition zones [155]. These micromechanical properties can be further used as input for the *meso*-scale modelling of mortar and concrete. However, it should be pointed out that the nanoindenter is a load-controlled instrument so that it is not possible to measure the behaviour after the peak load. Therefore, more advanced instruments are still required for the fracture test. Moreover, cantilever beams (length: 1.65 mm cross-section: 380 μm × 380 μm) can be prepared [156]. The indenter is able to perform the cyclic loads and sustained loads for the fatigue and creep test at the micro-scale [156,157]. This would offer more insight into the mechanism of fatigue and creep and facilitate developing more fundamental models.

6. Suggestions for further work

On the basis of the reviewed techniques related with micromechanical modelling of HCP, additional studies need to be performed in the future to obtain deeper insight into the microstructure-property relationship.

To simulate the realistic microstructure of HCP, more advanced hydration models are required. Such models should consider realistic cement particle shape and be built up on the basis of fundamental understanding of chemical kinetics at the molecular scale. Some preliminary work has already been reported in the literature [58,71,159–161], but there is still a significant need for the development.

With respect to the μ-CT generated microstructures, as standard segmentation approach does not exist, the segmented microstructures are not comparable when different segmentation approaches are used. On the one hand, quantitative studies on the influence of the segmentation approach on the obtained microstructures should be carried out. One the other hand, a possible way is to avoid the image segmentation process and direct use the original greyscale level based microstructures as input for the micromechanical modelling using the approaches presented in Ref. [144,146].

To model the fracture process of HCP, numerical models are suggested. However, it always requires a trade-off between accuracy and speed. As it is recommended to study the micromechanical properties of HCP in a statistical way, significant computational efforts are demanded. More power computational facilities and a more efficient numerical algorithm are needed in the future.

To assess the strength properties of individual phases in HCP as input for the micromechanical modelling, both experimental and numerical studies are required. In terms of experimental work, testing approaches like micro-bending and micro-pillar compression are recommended, because these approaches are able to provide strength properties. Considering the heterogeneous nature of HCP, more experimental measurements are required to provide statistically reliable results. Furthermore, various specimen geometries and loading conditions are required e.g., the uniaxial tension test which can be achieved using the set-up reported in Ref. [162]. Additionally, the results of nano-scale modelling offer interesting and promising prospects. However, as a big gap exists between nano- and micro-scales, models at sub-micro scale need to be developed to bridge such gap.

Although some preliminary work has been reported, more advanced mechanical testing approaches are required for the purpose of calibration and validation of micromechanical models. A system that is able to measure the post-peak behaviour and visualize the fracture process during loading would be beneficial to assess whether HCP actually shows quasi-brittle behaviour at micro-scale, as some models suggest. If so, the softening post-behaviour need to be measured as well. Use of in-situ experiments (such as X-CT in situ) which can monitor the fracture process of HCP during loading would offer the opportunity for further validate the models in terms of fracture performance. An attempt has been done by Trtik et al. [163]. However, the resolution of the whole setup was not quite sufficient to reveal much of the pre-peak fracture process, which was the actual goal of the experiment. Moreover, it is emphasized that, the calibration and validation can only be done when same size and shape specimens and loading conditions are used in the simulation and experiment. The measurements from a few centimetres sized specimens cannot be directly used for this purpose because different material structure features are presented at micro- and *meso*-scales [147,149].

In the future, it would be beneficial to use micromechanical models to explain the observations of time dependent behaviour of cementitious materials, such as shrinkage, creep, or fatigue, see Ref. [156]. For this purpose, multi-scale modelling is required. Concurrent approach or hierarchical approach is commonly adopted. These methods were initially based on two main concepts: scale separation and RVE [164–166]. As cementitious materials are heterogeneous at all length scales, experimental validations are suggested to be done at all length scales.

The techniques available for investigating the properties of HPC can be further developed for understanding the relationship between microstructure and properties of blended cementitious binders [145]. Both the models and the experimental scans can be used together to obtain the realistic microstructure of blended cementitious binders based on which its mechanical properties can be estimated. This helps designing cementitious materials with improved properties from the bottom up.

7. Conclusions

This paper provides an overview of aspects that related with the micromechanical modelling of cementitious materials. Based on the above discussions, the following conclusions can be drawn:

- Prediction of micromechanical behaviour of cementitious material requires well-characterised material structures, proper input parameters, and advanced fracture modelling approaches.
- For the material structure characterisation, numerical cement hydration models have clear advantages in terms of the efficiency, while the experimental approach is still more realistic. With recent advanced micro CT techniques, it is possible to

obtain a 3D microstructure of cementitious materials with a high resolution for the modelling of fracture performance of cementitious material at the micro-scale.

- Mechanical properties of individual phases are essential for the prediction of mechanical response of cement paste at the micro-scale. The elastic properties of these phases can be derived from the nanoindentation test or atomistic simulations. However, there remains a challenge when dealing with the strength characterization. Although pioneering work has been conducted, there remains significant research need in the prediction and measuring of the fracture properties of these phases.
- Several models have been proposed and implemented for the prediction of micromechanical properties of cement paste. The homogenization approaches are applicable for the prediction evolution of elastic properties along hydrating because of their high efficiency, but they cannot be used for fracture analysis. Discrete model have a clear advantage in this aspect. Stress/strain response of HCP predicted using different approaches shows large differences. Thus, fracture tests at the micro-scale are needed to calibrate the input parameters and validate the predicted micromechanical properties. Moreover, considering the heterogonous nature of the HCPs, it is recommended to perform the investigation in a statistic way.

Therefore, an experimentally validated modelling scheme is required for fundamental understanding and reliable prediction of the micromechanical properties of cementitious materials. To achieve this, advanced techniques in different fields need to be carefully selected and combined. Further work is needed in the part of experimental calibration and validation of the micromechanical models through advanced micromechanical measurements. These micromechanical testing and modelling approaches can be further developed for understanding the mechanical properties and fracture mechanisms of other binder materials. Such as blended cement pastes, geopolymer and recycled materials which are important for a sustainable future.

Declaration of Competing Interest

The authors declare that they have no known competing financial interests or personal relationships that could have appeared to influence the work reported in this paper.

Acknowledgement

References

[1] T.C. Powers, T.L. Brownyard, Studies of the physical properties of hardened Portland cement paste, J. Proceed. (1946) 101–132.
[2] H.A. Toutanji, T. El-Korchi, The influence of silica fume on the compressive strength of cement paste and mortar, Cem. Concr. Res. 25 (7) (1995) 1591–1602.
[3] T.J. Hirsch, Modulus of elasticity iof concrete affected by elastic moduli of cement paste matrix and aggregate, J. Proceed. (1962) 427–452.
[4] K.L. Scrivener, Backscattered electron imaging of cementitious microstructures: understanding and quantification, Cem. Concr. Compos. 26 (8) (2004) 935–945.
[5] E. Gallucci, K. Scrivener, A. Groso, M. Stampanoni, G. Margaritondo, 3D experimental investigation of the microstructure of cement pastes using synchrotron X-ray microtomography (μCT), Cem. Concr. Res. 37 (3) (2007) 360–368.
[6] K. Van Breugel, Simulation of hydration and formation of structure in hardening cement-based materials, Delft University of Technology, Delft, The Netherlands, 1991.
[7] E.A.B. Koenders, Simulation of volume changes in hardening cement-based materials, TU Delft, Delft University of Technology, 1997.
[8] G. Ye, Experimental study and numerical simulation of the development of the microstructure and permeability of cementitious materials, (2003).
[9] S. Bishnoi, Vector modelling of hydrating cement microstructure and kinetics, (2008).
[10] S. Bishnoi, K.L. Scrivener, μic: A new platform for modelling the hydration of cements, Cem. Concr. Res. 39 (4) (2009) 266–274.
[11] D.P. Bentz, Three-dimensional computer simulation of portland cement hydration and microstructure development, J. Am. Ceram. Soc. 80 (1) (1997) 3–21.
[12] C. Hu, Z. Li, Micromechanical investigation of Portland cement paste, Constr. Build. Mater. 71 (2014) 44–52.
[13] G. Constantinides, F.-J. Ulm, The effect of two types of CSH on the elasticity of cement-based materials: Results from nanoindentation and micromechanical modeling, Cem. Concr. Res. 34 (1) (2004) 67–80.
[14] H.M. Jennings, J.J. Thomas, J.S. Gevrenov, G. Constantinides, F.-J. Ulm, A multi-technique investigation of the nanoporosity of cement paste, Cem. Concr. Res. 37 (3) (2007) 329–336.
[15] J.J. Hughes, P. Trtik, Micro-mechanical properties of cement paste measured by depth-sensing nanoindentation: a preliminary correlation of physical properties with phase type, Mater. Charact. 53 (2) (2004) 223–231.
[16] H. Manzano, J. Dolado, A. Guerrero, A. Ayuela, Mechanical properties of crystalline calcium-silicate-hydrates: comparison with cementitious C-S-H gels, Phys. Status Solidi (A) 204 (6) (2007) 1775–1780.
[17] R.J.-M. Pellenq, A. Kushima, R. Shahsavari, K.J. Van Vliet, M.J. Buehler, S. Yip, F.-J. Ulm, A realistic molecular model of cement hydrates, Proc. Natl. Acad. Sci. 106 (38) (2009) 16102–16107.
[18] M.H.N. Yio, M.J. Mac, H.S. Wong, N.R. Buenfeld, 3D imaging of cement-based materials at submicron resolution by combining laser scanning confocal microscopy with serial sectioning, JMic 258 (2) (2015) 151–169.
[19] M.K. Head, N.R. Buenfeld, Confocal imaging of porosity in hardened concrete, Cem. Concr. Res. 36 (5) (2006) 896–911.
[20] L. Holzer, P. Gasser, A. Kaech, M. Wegmann, A. Zingg, R. Wepf, B. Muench, Cryo-FIB-nanotomography for quantitative analysis of particle structures in cement suspensions, JMic 227 (3) (2007) 216–228.
[21] P. Trtik, B. Münch, P. Gasser, A. Leemann, R. Loser, R. Wepf, P. Lura, Focussed ion beam nanotomography reveals the 3D morphology of different solid phases in hardened cement pastes, JMic 241 (3) (2011) 234–242.
[22] S.R. Chae, J. Moon, S. Yoon, S. Bae, P. Levitz, R. Winarski, P.J. Monteiro, Advanced nanoscale characterization of cement based materials using X-ray synchrotron radiation: a review, Int. J. Concr. Struct. Mater. 7 (2) (2013) 95–110.
[23] J. Ha, S. Chae, K. Chou, T. Tyliszczak, P. Monteiro, Effect of polymers on the nanostructure and on the carbonation of calcium silicate hydrates: a scanning transmission X-ray microscopy study, J. Mater. Sci. 47 (2) (2012) 976–989.
[24] J.I. Goldstein, D.E. Newbury, J.R. Michael, N.W. Ritchie, J.H.J. Scott, D.C. Joy, Scanning electron microscopy and X-ray microanalysis, Springer, 2017.
[25] K.L. Scrivener, H. Patel, P. Pratt, L. Parrott, Analysis of phases in cement paste using backscattered electron images, methanol adsorption and thermogravimetric analysis, MRS Online Proceed. Lib. Arch. 85 (1986).
[26] H. Wong, M. Head, N. Buenfeld, Pore segmentation of cement-based materials from backscattered electron images, Cem. Concr. Res. 36 (6) (2006) 1083–1090.
[27] J. Němeček, V. Králík, V. Šmilauer, L. Polívka, A. Jäger, Tensile strength of hydrated cement paste phases assessed by micro-bending tests and nanoindentation, Cem. Concr. Compos. 73 (2016) 164–173.
[28] A. Michel, B.J. Pease, M.R. Geiker, H. Stang, J.F. Olesen, Monitoring reinforcement corrosion and corrosion-induced cracking using non-destructive x-ray attenuation measurements, Cem. Concr. Res. 41 (11) (2011) 1085–1094.
[29] M. Souza, L.C. Pardini, E.C. Botelho, M. Costa, X-ray tomography applied to the void/defect measurement of hybrid CFRC/SiC composites, Mater. Res. Express (2018).
[30] C. Hall, S.L. Colston, A.C. Jupe, S.D. Jacques, R. Livingston, A.O. Ramadan, A.W. Amde, P. Barnes, Non-destructive tomographic energy-dispersive diffraction imaging of the interior of bulk concrete, Cem. Concr. Res. 30 (3) (2000) 491–495.
[31] T. Chotard, M. Boncoeur-Martel, A. Smith, J. Dupuy, C. Gault, Application of X-ray computed tomography to characterise the early hydration of calcium aluminate cement, Cem. Concr. Compos. 25 (1) (2003) 145–152.
[32] F. Auzerais, J. Dunsmuir, B. Ferreol, N. Martys, J. Olson, T. Ramakrishnan, D. Rothman, L. Schwartz, Transport in sandstone: A study based on three dimensional microtomography, GeoRL 23 (7) (1996) 705–708.
[33] E. Rosenberg, J. Lynch, P. Gueroult, M. Bisiaux, R.F. De Paiva, High resolution 3D reconstructions of rocks and composites, Oil & Gas Sci. Technol. 54 (4) (1999) 497–511.
[34] T.-S. Han, X. Zhang, J.-S. Kim, S.-Y. Chung, J.-H. Lim, C. Linder, Area of lineal-path function for describing the pore microstructures of cement paste and their relations to the mechanical properties simulated from μ-CT microstructures, Cem. Concr. Compos. 89 (2018) 1–17.

[35] M.A.B. Promentilla, T. Sugiyama, T. Hitomi, N. Takeda, Quantification of tortuosity in hardened cement pastes using synchrotron-based X-ray computed microtomography, Cem. Concr. Res. 39 (6) (2009) 548–557.

[36] M.Z. Zhang, Y.J. He, G. Ye, D.A. Lange, K. van Breugel, Computational investigation on mass diffusivity in Portland cement paste based on X-ray computed microtomography (mu CT) image, Constr. Build. Mater. 27 (1) (2012) 472–481.

[37] D.P. Bentz, S. Mizell, S. Satterfield, J. Devaney, W. George, P. Ketcham, J. Graham, J. Porterfield, D. Quenard, F. Vallee, The visible cement data set, J. Res. Nat. Inst. Stand. Technol. 107 (2) (2002) 137.

[38] H. Zhang, B. Šavija, S. Chaves Figueiredo, M. Lukovic, E. Schlangen, Microscale testing and modelling of cement paste as basis for multi-scale modelling, Materials 9 (11) (2016) 907.

[39] B. Šavija, H. Zhang, E. Schlangen, Assessing hydrated cement paste properties using experimentally informed discrete models, J. Mater. Civ. Eng. 31 (9) (2019) 04019169.

[40] H. Zhang, E. Schlangen, B. Šavija, Testing and modelling of micro cement paste cube under indentation splitting, Computational Modelling of Concrete Structures: Proceedings of the Conference on Computational Modelling of Concrete and Concrete Structures (EURO-C 2018), February 26-March 1, 2018, Bad Hofgastein, Austria, CRC Press, 2018, p. 121.

[41] H. Zhang, B. Šavija, E. Schlangen, Towards understanding stochastic fracture performance of cement paste at micro length scale based on numerical simulation, Constr. Build. Mater. 183 (2018) 189–201.

[42] N. Bossa, P. Chaurand, J. Vicente, D. Borschneck, C. Levard, O. Aguerre-Chariol, J. Rose, Micro-and nano-X-ray computed-tomography: A step forward in the characterization of the pore network of a leached cement paste, Cem. Concr. Res. 67 (2015) 138–147.

[43] J.-S. Kim, S.-Y. Chung, D. Stephan, T.-S. Han, Issues on characterization of cement paste microstructures from µ-CT and virtual experiment framework for evaluating mechanical properties, Constr. Build. Mater. 202 (2019) 82–102.

[44] M. Zhang, A.P. Jivkov, Microstructure-informed modelling of damage evolution in cement paste, Constr. Build. Mater. 66 (2014) 731–742.

[45] M. Zhang, A.P. Jivkov, Micromechanical modelling of deformation and fracture of hydrating cement paste using X-ray computed tomography characterisation, Compos. B Eng. 88 (2016) 64–72.

[46] M. Hain, P. Wriggers, Numerical homogenization of hardened cement paste, CompM 42 (2) (2008) 197–212.

[47] M. Zhang, G. Ye, K. Van Breugel, Microstructure-based modeling of water diffusivity in cement paste, Constr. Build. Mater. 25 (4) (2011) 2046–2052.

[48] K. Van Breugel, Modelling of cement-based systems—the alchemy of cement chemistry, Cem. Concr. Res. 34 (9) (2004) 1661–1668.

[49] C. Pignat, P. Navi, K. Scrivener, Simulation of cement paste microstructure hydration, pore space characterization and permeability determination, Mater. Struct. 38 (4) (2005) 459–466.

[50] J.S. Dolado, K. Van Breugel, Recent advances in modeling for cementitious materials, Cem. Concr. Res. 41 (7) (2011) 711–726.

[51] J.J. Thomas, J.J. Biernacki, J.W. Bullard, S. Bishnoi, J.S. Dolado, G.W. Scherer, A. Luttge, Modeling and simulation of cement hydration kinetics and microstructure development, Cem. Concr. Res. 41 (12) (2011) 1257–1278.

[52] P. Gao, Simulation of hydration and microstructure development of blended cements, Delft University of Technology, PhD Thesis. Delft, The Netherlands, 2018.

[53] H.M. Jennings, S.K. Johnson, Simulation of microstructure development during the hydration of a cement compound, J. Am. Ceram. Soc. 69 (11) (1986) 790–795.

[54] P. Navi, C. Pignat, Simulation of cement hydration and the connectivity of the capillary pore space, Adv. Cem. Based Mater. 4 (2) (1996) 58–67.

[55] R. Nothnagel, H. Budelmann, Model for the formation of microstructure in cement paste during hydration, International RILEM Symposium on Concrete Modelling-ConMod'08, RILEM Publications SARL (2008) 361–368.

[56] X.-Y. Wang, H.-S. Lee, K.-B. Park, Simulation of low-calcium fly ash blended cement hydration, ACI Mater. J. 106 (2) (2009) 167.

[57] K. Maekawa, R. Chaube, T. Kishi, Modeling of concrete performance: hydration, microstructure formation and mass transport, E and FN SPON, London 1 (1999).

[58] J.W. Bullard, A three-dimensional microstructural model of reactions and transport in aqueous mineral systems, Modell. Simul. Mater. Sci. Eng. 15 (7) (2007) 711.

[59] L. Liu, X. Wang, H. Chen, C. Wan, Microstructure-based modelling of drying shrinkage and microcracking of cement paste at high relative humidity, Constr. Build. Mater. 126 (2016) 410–425.

[60] Z. Qian, Multiscale modeling of fracture processes in cementitious materials, Delft University of Technology, Delft, The Netherlands, 2012.

[61] R. Chamrova, Modelling and measurement of elastic properties of hydrating cement paste, (2010).

[62] Q.H. Do, Modelling Properties of Cement Paste from Microstructure, (2013).

[63] S. Bishnoi, S. Joseph, A. Kaur, Microstructural modelling of the strength of mortars containing fly ash using µic, Constr. Build. Mater. 163 (2018) 912–920.

[64] J.W. Bullard, E.J. Garboczi, A model investigation of the influence of particle shape on portland cement hydration, Cem. Concr. Res. 36 (6) (2006) 1007–1015.

[65] B. Pichler, C. Hellmich, J. Eberhardsteiner, Spherical and acicular representation of hydrates in a micromechanical model for cement paste: prediction of early-age elasticity and strength, AcMec 203 (3) (2009) 137–162.

[66] E.J. Garboczi, J.W. Bullard, Shape analysis of a reference cement, Cem. Concr. Res. 34 (10) (2004) 1933–1937.

[67] J. Sanahuja, L. Dormieux, G. Chanvillard, Modelling elasticity of a hydrating cement paste, Cem. Concr. Res. 37 (10) (2007) 1427–1439.

[68] C.-J. Haecker, E. Garboczi, J. Bullard, R. Bohn, Z. Sun, S.P. Shah, T. Voigt, Modeling the linear elastic properties of Portland cement paste, Cem. Concr. Res. 35 (10) (2005) 1948–1960.

[69] D.P. Bentz, O.M. Jensen, K.K. Hansen, J.F. Olesen, H. Stang, C.J. Haecker, Influence of cement particle-size distribution on early age autogenous strains and stresses in cement-based materials, J. Am. Ceram. Soc. 84 (1) (2001) 129–135.

[70] J. Von Neumann, A.W. Burks, Theory of self-reproducing automata, ITNN 5 (1) (1966) 3–14.

[71] J.W. Bullard, Approximate rate constants for nonideal diffusion and their application in a stochastic model, J. Phys. Chem. A 111 (11) (2007) 2084–2092.

[72] F. Bernard, S. Kamali-Bernard, Predicting the evolution of mechanical and diffusivity properties of cement pastes and mortars for various hydration degrees–a numerical simulation investigation, Comput. Mater. Sci. 61 (2012) 106–115.

[73] W.C. Oliver, G.M. Pharr, An improved technique for determining hardness and elastic modulus using load and displacement sensing indentation experiments, J. Mater. Res. 7 (6) (1992) 1564–1583.

[74] H. Hertz, D.E. Jones, G.A. Schott, Miscellaneous papers, Macmillan and Company, 1896.

[75] C. Hu, Z. Li, A review on the mechanical properties of cement-based materials measured by nanoindentation, Constr. Build. Mater. 90 (2015) 80–90.

[76] J. Woirgard, C. Tromas, J. Girard, V. Audurier, Study of the mechanical properties of ceramic materials by the nanoindentation technique, J. Eur. Ceram. Soc. 18 (15) (1998) 2297–2305.

[77] A. Shimamoto, K. Tanaka, Y. Akiyma, H. Yoshizaki, Nanoindentation of glass with a tip-truncated Berkovich indenter, Philos. Mag. A 74 (5) (1996) 1097–1105.

[78] C. Hu, Y. Gao, Y. Zhang, Z. Li, Statistical nanoindentation technique in application to hardened cement pastes: Influences of material microstructure and analysis method, Constr. Build. Mater. 113 (2016) 306–316.

[79] H. Bückle, Use of the hardness test to determine other material properties, The Science of Hardness Testing and Its Research Applications (1973) 453.

[80] J.J. Chen, L. Sorelli, M. Vandamme, F.J. Ulm, G. Chanvillard, A Coupled Nanoindentation/SEM-EDS Study on Low Water/Cement Ratio Portland Cement Paste: Evidence for C-S-H/Ca (OH) 2 Nanocomposites, J. Am. Ceram. Soc. 93 (5) (2010) 1484–1493.

[81] G. Constantinides, F.-J. Ulm, The nanogranular nature of C-S-H, J. Mech. Phys. Solids 55 (1) (2007) 64–90.

[82] G. Constantinides, F.-J. Ulm, K. Van Vliet, On the use of nanoindentation for cementitious materials, Mater. Struct. 36 (3) (2003) 191–196.

[83] F.J. Ulm, M. Vandamme, C. Bobko, J. Alberto Ortega, K. Tai, C. Ortiz, Statistical indentation techniques for hydrated nanocomposites: concrete, bone, and shale, J. Am. Ceram. Soc. 90 (9) (2007) 2677–2692.

[84] M. Miller, C. Bobko, M. Vandamme, F.-J. Ulm, Surface roughness criteria for cement paste nanoindentation, Cem. Concr. Res. 38 (4) (2008) 467–476.

[85] D. Davydov, M. Jirásek, L. Kopecký, Critical aspects of nano-indentation technique in application to hardened cement paste, Cem. Concr. Res. 41 (1) (2011) 20–29.

[86] P. Lura, P. Trtik, B. Münch, Validity of recent approaches for statistical nanoindentation of cement pastes, Cem. Concr. Compos. 33 (4) (2011) 457–465.

[87] F.-J. Ulm, M. Vandamme, H.M. Jennings, J. Vanzo, M. Bentivegna, K.J. Krakowiak, G. Constantinides, C.P. Bobko, K.J. Van Vliet, Does microstructure matter for statistical nanoindentation techniques?, Cem Concr. Compos. 32 (1) (2010) 92–99.

[88] P. Trtik, B. Münch, P. Lura, A critical examination of statistical nanoindentation on model materials and hardened cement pastes based on virtual experiments, Cem. Concr. Compos. 31 (10) (2009) 705–714.

[89] M. Luković, E. Schlangen, G. Ye, Combined experimental and numerical study of fracture behaviour of cement paste at the microlevel, Cem. Concr. Res. 73 (2015) 123–135.

[90] K. Velez, S. Maximilien, D. Damidot, G. Fantozzi, F. Sorrentino, Determination by nanoindentation of elastic modulus and hardness of pure constituents of Portland cement clinker, Cem. Concr. Res. 31 (4) (2001) 555–561.

[91] W. Zhu, J.J. Hughes, N. Bicanic, C.J. Pearce, Nanoindentation mapping of mechanical properties of cement paste and natural rocks, Mater. Charact. 58 (11) (2007) 1189–1198.

[92] M. Vandamme, F.-J. Ulm, Nanogranular origin of concrete creep, Proc. Natl. Acad. Sci. 106 (26) (2009) 10552–10557.

[93] M. Vandamme, F.-J. Ulm, Nanoindentation investigation of creep properties of calcium silicate hydrates, Cem. Concr. Res. 52 (2013) 38–52.

[94] T. Howind, J. Hughes, W. Zhu, F. Puertas, S. Goñi Elizalde, M.S. Hernandez, A. Guerrero Bustos, M. Palacios, J.S. Dolado, Mapping of mechanical properties of cement paste microstructures, (2011).

[95] S.J. Chen, W.H. Duan, Z.J. Li, T.B. Sui, New approach for characterisation of mechanical properties of cement paste at micrometre scale, Mater. Des. 87 (2015) 992–995.

[96] R. Shahrin, C.P. Bobko, Characterizing strength and failure of calcium silicate hydrate aggregates in cement paste under micropillar compression, J. Nanomech. Micromech. 7 (4) (2017) 06017002.

[97] R. Shahrin, C.P. Bobko, Micropillar compression investigation of size effect on microscale strength and failure mechanism of Calcium-Silicate-Hydrates (C-S-H) in cement paste, Cem. Concr. Res. 125 (2019) 105863.

[98] M.J. Pfeifenberger, M. Mangang, S. Wurster, J. Reiser, A. Hohenwarter, W. Pfleging, D. Kiener, R. Pippan, The use of femtosecond laser ablation as a novel tool for rapid micro-mechanical sample preparation, Mater. Des. 121 (2017) 109–118.

[99] B. Šavija, D. Liu, G. Smith, K.R. Hallam, E. Schlangen, P.E. Flewitt, Experimentally informed multi-scale modelling of mechanical properties of quasi-brittle nuclear graphite, Eng. Fract. Mech. 153 (2016) 360–377.

[100] J. Němeček, J. Maňák, T. Krejčí, Effect of vacuum and Focused Ion Beam generated heat on fracture properties of hydrated cement paste, Cem. Concr. Compos. 100 (2019) 139–149.

[101] H. Manzano, J. Dolado, A. Ayuela, Elastic properties of the main species present in Portland cement pastes, Acta Mater. 57 (5) (2009) 1666–1674.

[102] D. Tavakoli, A. Tarighat, Molecular dynamics study on the mechanical properties of Portland cement clinker phases, Comput. Mater. Sci. 119 (2016) 65–73.

[103] H. Manzano, J.S. Dolado, A. Ayuela, Structural, mechanical, and reactivity properties of tricalcium aluminate using first-principles calculations, J. Am. Ceram. Soc. 92 (4) (2009) 897–902.

[104] D. Grigoratos, J. Knowles, Y.L. Ng, K. Gulabivala, Effect of exposing dentine to sodium hypochlorite and calcium hydroxide on its flexural strength and elastic modulus, Int. Endod. J. 34 (2) (2001) 113–119.

[105] A.G. Kalinichev, R.J. Kirkpatrick, Molecular dynamics modeling of chloride binding to the surfaces of calcium hydroxide, hydrated calcium aluminate, and calcium silicate phases, Chem. Mater. 14 (8) (2002) 3539–3549.

[106] A.G. Kalinichev, J. Wang, R.J. Kirkpatrick, Molecular dynamics modeling of the structure, dynamics and energetics of mineral–water interfaces: Application to cement materials, Cem. Concr. Res. 37 (3) (2007) 337–347.

[107] S.V. Churakov, Hydrogen bond connectivity in jennite from ab initio simulations, Cem. Concr. Res. 38 (12) (2008) 1359–1364.

[108] S.V. Churakov, Structural position of H2O molecules and hydrogen bonding in anomalous 11 A tobermorite, Am Min 94 (1) (2009) 156–165.

[109] S.V. Churakov, Structure of the interlayer in normal 11 A tobermorite from an ab initio study, Eur. J. Mineral. 21 (1) (2009) 261–271.

[110] R. Shahsavari, M.J. Buehler, R.J.M. Pellenq, F.J. Ulm, First-principles study of elastic constants and interlayer interactions of complex hydrated oxides: Case study of tobermorite and jennite, J. Am. Ceram. Soc. 92 (10) (2009) 2323–2330.

[111] H. Manzano, R. González-Teresa, J. Dolado, A. Ayuela, X-ray spectra and theoretical elastic properties of crystalline calcium silicate hydrates: comparison with cement hydrated gels, Mater. de Constr. 60 (299) (2010) 7–19.

[112] D. Hou, Y. Zhu, Y. Lu, Z.J.M.C. Li, Physics, Mechanical properties of calcium silicate hydrate (C–S–H) at nano-scale: a molecular dynamics study, 146(3) (2014) 503-511

[113] D. Hou, H. Ma, Y. Zhu, Z.J.A.m. Li, Calcium silicate hydrate from dry to saturated state: structure, dynamics and mechanical properties, 67 (2014) 81-94.

[114] D. Hou, J. Yu, P.J.C.P.B.E. Wang, Molecular dynamics modeling of the structure, dynamics, energetics and mechanical properties of cement-polymer nanocomposite, 162 (2019) 433-444.

[115] D. Hou, J. Zhang, W. Pan, Y. Zhang, Z.J.J.o.N.M. Zhang, Nanoscale mechanism of ions immobilized by the geopolymer: A molecular dynamics study, 528 (2020) 151841.

[116] D. Hou, T. Zhao, H. Ma, Z.J.T.J.o.P.C.C. Li, Reactive molecular simulation on water confined in the nanopores of the calcium silicate hydrate gel: structure, reactivity, and mechanical properties, 119(3) (2015) 1346-1358.

[117] H.M. Jennings, Refinements to colloid model of CSH in cement: CM-II, Cem. Concr. Res. 38 (3) (2008) 275–289.

[118] H.M. Jennings, A model for the microstructure of calcium silicate hydrate in cement paste, Cem. Concr. Res. 30 (1) (2000) 101–116.

[119] R. Gonzalez-Teresa, V. Morales-Florez, H. Manzano, J.S. Dolado, Structural models of randomly packed Tobermorite-like spherical particles: A simple computational approach, Mater. de constr. 60 (298) (2010) 7–15.

[120] V. Morales-Florez, F. Brunet, Structural models of random packing of spheres extended to bricks: simulation of the nanoporous calcium silicate hydrates, MoSim 35 (12–13) (2009) 1001–1006.

[121] V. Morales-Flórez, N. De La Rosa-Fox, M. Piñero, L. Esquivias, The cluster model: a simulation of the aerogel structure as a hierarchically-ordered arrangement of randomly packed spheres, JSGST 35 (3) (2005) 203–210.

[122] D.P. Bentz, D.A. Quenard, V. Baroghel-Bouny, E.J. Garboczi, H.M. Jennings, Modelling drying shrinkage of cement paste and mortar Part 1. Structural models from nanometres to millimetres, Materials and Structures 28(8) (1995) 450-458.

[123] M.Q. Chandler, J.F. Peters, D. Pelessone, Modeling nanoindentation of calcium silicate hydrate, Transp. Res. Rec. 2142 (1) (2010) 67–74.

[124] F. Sanchez, K. Sobolev, Nanotechnology in concrete–a review, Constr. Build. Mater. 24 (11) (2010) 2060–2071.

[125] R.M. Jones, Mechanics of composite materials, CRC press2014.

[126] Y. Benveniste, A new approach to the application of Mori-Tanaka's theory in composite materials, Mech. Mater. 6 (2) (1987) 147–157.

[127] B. Budiansky, On the elastic moduli of some heterogeneous materials, J. Mech. Phys. Solids 13 (4) (1965) 223–227.

[128] O. Bernard, F.-J. Ulm, E. Lemarchand, A multiscale micromechanics-hydration model for the early-age elastic properties of cement-based materials, Cem. Concr. Res. 33 (9) (2003) 1293–1309.

[129] B. Pichler, S. Scheiner, C. Hellmich, From micron-sized needle-shaped hydrates to meter-sized shotcrete tunnel shells: micromechanical upscaling of stiffness and strength of hydrating shotcrete, Acta Geotech. 3 (4) (2008) 273.

[130] B. Pichler, C. Hellmich, Upscaling quasi-brittle strength of cement paste and mortar: A multi-scale engineering mechanics model, Cem. Concr. Res. 41 (5) (2011) 467–476.

[131] M. Hlobil, V. Šmilauer, G. Chanvillard, Micromechanical multiscale fracture model for compressive strength of blended cement pastes, Cem. Concr. Res. 83 (2016) 188–202.

[132] Q. Chen, Z. Jiang, Z. Yang, H. Zhu, J.W. Ju, Z. Yan, Y.J.M. Wang, structures, Differential-scheme based micromechanical framework for saturated concrete repaired by the electrochemical deposition method, 49(12) (2016) 5183-5193.

[133] H. Zhu, Q. Chen, J.W. Ju, Z. Yan, F. Guo, Y. Wang, Z. Jiang, S. Zhou, B.J.A.M. Wu, Maximum entropy-based stochastic micromechanical model for a two-phase composite considering the inter-particle interaction effect, 226(9) (2015) 3069-3084.

[134] E.J. Garboczi, A. Day, An algorithm for computing the effective linear elastic properties of heterogeneous materials: three-dimensional results for composites with equal phase Poisson ratios, J. Mech. Phys. Solids 43 (9) (1995) 1349–1362.

[135] P. Wriggers, M. Hain, Micro-meso-macro modelling of composite materials, Springer, Computational Plasticity, 2007, pp. 105–122.

[136] V. Šmilauer, Z. Bittnar, Microstructure-based micromechanical prediction of elastic properties in hydrating cement paste, Cem. Concr. Res. 36 (9) (2006) 1708–1718.

[137] E. Stora, Q.C. He, B. Bary, Influence of inclusion shapes on the effective linear elastic properties of hardened cement pastes, Cem. Concr. Res. 36 (7) (2006) 1330–1344.

[138] B. Bary, M.B. Haha, E. Adam, P. Montarnal, Numerical and analytical effective elastic properties of degraded cement pastes, Cem. Concr. Res. 39 (10) (2009) 902–912.

[139] F. Bernard, S. Kamali-Bernard, W. Prince, 3D multi-scale modelling of mechanical behaviour of sound and leached mortar, Cem. Concr. Res. 38 (4) (2008) 449–458.

[140] E. Schlangen, E. Garboczi, Fracture simulations of concrete using lattice models: computational aspects, Eng. Fract. Mech. 57 (2) (1997) 319–332.

[141] E. Schlangen, Experimental and numerical analysis of fracture processes in concrete, Delft University of Technology, 1993.

[142] C. Lee, X. Wei, J.W. Kysar, J. Hone, Measurement of the elastic properties and intrinsic strength of monolayer graphene, science 321(5887) (2008) 385-388.

[143] A.A. Griffith, The phenomena of rupture and flow in solids, Philosophical transactions of the royal society of london. Series A, containing papers of a mathematical or physical character 221 (1921) 163-198.

[144] H. Zhang, B. Šavija, M. Luković, E. Schlangen, Experimentally informed micromechanical modelling of cement paste: An approach coupling X-ray computed tomography and statistical nanoindentation, Compos. B Eng. 157 (2019) 109–122.

[145] B. Šavija, H. Zhang, E.J.C. Schlangen, B. Materials, Micromechanical testing and modelling of blast furnace slag cement pastes, 239 (2020) 117841.

[146] S. Monfared, H. Laubie, F. Radjai, M. Hubler, R. Pellenq, F.-J. Ulm, A methodology to calibrate and to validate effective solid potentials of heterogeneous porous media from computed tomography scans and laboratory-measured nanoindentation data, Acta Geotech. 13 (6) (2018) 1371–1394.

[147] H. Zhang, B. Šavija, S.C. Figueiredo, E. Schlangen, Experimentally validated multi-scale modelling scheme of deformation and fracture of cement paste, Cem. Concr. Res. 102 (2017) 175–186.

[148] H. Ma, D. Hou, Y. Lu, Z. Li, Two-scale modeling of the capillary network in hydrated cement paste, Constr. Build. Mater. 64 (2014) 11–21.

[149] H. Zhang, B. Šavija, Y. Xu, E. Schlangen, Size effect on splitting strength of hardened cement paste: Experimental and numerical study, Cem. Concr. Compos. 94 (2018) 264–276.

[150] Z.P. Bažant, S.-D. Pang, Activation energy based extreme value statistics and size effect in brittle and quasibrittle fracture, J. Mech. Phys. Solids 55 (1) (2007) 91–131.

[151] A. Carpinteri, S. Puzzi, Fractals, statistics and size-scale effects on concrete strength, Fract. Mech. Concr. Struct. (2007) 31–37.

[152] H. Zhang, B. Šavija, E. Schlangen, Combined experimental and numerical study on micro-cube indentation splitting test of cement paste, Eng. Fract. Mech. (2018).

[153] H. Zhang, Y. Xu, Y. Gan, Z. Chang, E. Schlangen, B. Šavija, Combined experimental and numerical study of uniaxial compression failure of hardened cement paste at micrometre length scale, Cem. Concr. Res. 126 (2019) 105925.

[154] J.G. Van Mier, Concrete fracture: a multiscale approach, CRC press2012.

[155] H. Zhang, Y. Gan, Y. Xu, S. Zhang, E. Schlangen, B. Šavija, Experimentally informed fracture modelling of interfacial transition zone at micro-scale, Cem. Concr. Compos. 103383 (2019).

[156] Y. Gan, H. Zhang, B. Šavija, E. Schlangen, K. van Breugel, Static and fatigue tests on cementitious cantilever beams using nanoindenter, Micromachines 9 (12) (2018) 630.

[157] Y. Gan, H. Zhang, B. Šavija, E. Schlangen, K. van Breugel, G. Pijaudier-Cabot, P. Grassl, C. La Borderie, Micro-Cantilever Testing Of Cementitious Materials Under Various Loading Conditions, (2019).

[158] H. Zhang, B. Šavija, E. Schlangen, Combined experimental and numerical study on micro-cube indentation splitting test of cement paste, Eng. Fract. Mech. 199 (2018) 773–786.

[159] Y. Zuo, Z. Qian, E.J. Garboczi, G. Ye, Numerical simulation of the initial particle parking structure of cement/geopolymer paste and the dissolution of amorphous silica using real-shape particles, Constr. Build. Mater. 185 (2018) 206–219.

[160] S. Bishnoi, K.L. Scrivener, Studying nucleation and growth kinetics of alite hydration using µic, Cem. Concr. Res. 39 (10) (2009) 849–860.

[161] A. Ouzia, K. Scrivener, The needle model: A new model for the main hydration peak of alite, Cem. Concr. Res. 115 (2019) 339–360.

[162] Y. Kihara, T. Nagoshi, T.-F.M. Chang, H. Hosoda, S. Tatsuo, M. Sone, Tensile behavior of micro-sized specimen made of single crystalline nickel, MatL 153 (2015) 36–39.

[163] P. Trtik, P. Stähli, E. Landis, M. Stampanoni, J. Van Mier, Microtensile testing and 3D imaging of hydrated Portland cement, Proceedings 6th international conference on fracture mechanics of concrete and concrete structures (FraMCoS-VI), Taylor & Francis, London, 2007, pp. 1277–1282.

[164] P.J. Sánchez, P.J. Blanco, A.E. Huespe, R. Feijóo, Failure-oriented multi-scale variational formulation: micro-structures with nucleation and evolution of softening bands, Comput. Methods Appl. Mech. Eng. 257 (2013) 221–247.

[165] S. Eckardt, Adaptive heterogeneous multiscale models for the nonlinear simulation of concrete, (2009).

[166] I. Gitman, H. Askes, L. Sluys, Coupled-volume multi-scale modelling of quasi-brittle material, Eur. J. Mech. A/Solids 27 (3) (2008) 302–327.